



OPEN ACCESS

EDITED BY
Alessandro Maria Michetti,
University of Insubria, Italy

REVIEWED BY
Stella Maris Moreiras,
CONICET Mendoza, Argentina
Franz Livio,
University of Insubria, Italy
Luigi Piccardi,
National Research Council (CNR), Italy
Franck Audemard,
Central University of Venezuela,
Venezuela

*CORRESPONDENCE
Thomas K. Rockwell,
trockwell@sdsu.edu

SPECIALTY SECTION
This article was submitted to Structural
Geology and Tectonics,
a section of the journal
Frontiers in Earth Science

RECEIVED 30 August 2022
ACCEPTED 08 November 2022
PUBLISHED 14 December 2022

CITATION
Rockwell TK, Costa CH, Meigs AJ,
Ragona D, Owen LA, Murari MK,
Masana E and Richard AD (2022),
Paleoseismology of the Marquesado-La
Rinconada thrust system, Eastern
Precordillera of Argentina.
Front. Earth Sci. 10:1032357.
doi: 10.3389/feart.2022.1032357

COPYRIGHT
© 2022 Rockwell, Costa, Meigs, Ragona,
Owen, Murari, Masana and Richard. This
is an open-access article distributed
under the terms of the [Creative Commons Attribution License \(CC BY\)](https://creativecommons.org/licenses/by/4.0/).
The use, distribution or reproduction in
other forums is permitted, provided the
original author(s) and the copyright
owner(s) are credited and that the
original publication in this journal is
cited, in accordance with accepted
academic practice. No use, distribution
or reproduction is permitted which does
not comply with these terms.

Paleoseismology of the Marquesado-La Rinconada thrust system, Eastern Precordillera of Argentina

Thomas K. Rockwell^{1*}, Carlos H. Costa², Andrew J. Meigs³, Daniel Ragona^{1,4}, Lewis A. Owen⁵, Madhav Krishna Murari^{5,6}, Eulalia Masana⁷ and Andrés D. Richard²

¹Department of Geological Sciences, San Diego State University, San Diego, CA, United States, ²Departamento de Geología, Universidad Nacional de San Luis, San Luis, Argentina, ³College of Earth, Ocean and Atmospheric Sciences, Oregon State University, Corvallis, OR, United States, ⁴Ecopetrol, Bogota, Colombia, ⁵Department of Marine, Earth, and Atmospheric Sciences, North Carolina State University, Raleigh, NC, United States, ⁶Inter-University Accelerator Center, New Delhi, India, ⁷Dinàmica de la Terra i del Oceà, University of Barcelona, Barcelona, Spain

Excavated trenches at two sites across the Marquesado–La Rinconada fault system along the eastern Precordilleran front south of San Juan, Argentina, reveal the earthquake history of this rapidly urbanizing region. Interpretation of earthquakes is based on both the generation of colluvial wedges and upward fault terminations, as well as folding events in fine-grained alluvium ponded behind upslope-facing fault scarps. The ages of the past five interpreted earthquakes at the Loma Negra site are E1 at 2.8 ± 2.8 ka, E2 at 7.1 ± 1.5 ka, E3 at 9.6 ± 1.3 ka, E4 at 14.4 ± 2.1 ka, and E5 at 17.2 ± 3.1 ka. At the Jejenes sites, we documented event ages of 2.7 ± 0.1 ka, 3.9 ± 0.6 ka, 5.9 ± 1.3 ka, and 11.4 ± 4 ka. These results indicate that the recurrence interval along the Marquesado–La Rinconada fault zone averages several thousand years. The inferred displacements at the Jejenes site are about 1.1 m for E1, E3, and E4 and 2.1 m for event E2, whereas the displacements at Loma Negra averaged about 1 m, but the most recent event displays less slip. Notably, the older events seem to have been larger and emergent, whereas the youngest event appears to have been smaller and blind in the ponded sediment; this may partially explain the poor expression of classic colluvial wedges associated with some events. Despite the fact that active surface faulting has an uncertain relationship with the primary seismic sources at depth in the crust, past and future events of $M_w \sim 7.5$ are consistent with the length scale of active deformation, the $\sim 1\text{--}2$ m slip per event scale of these ruptures, and the size of historical earthquakes.

KEYWORDS

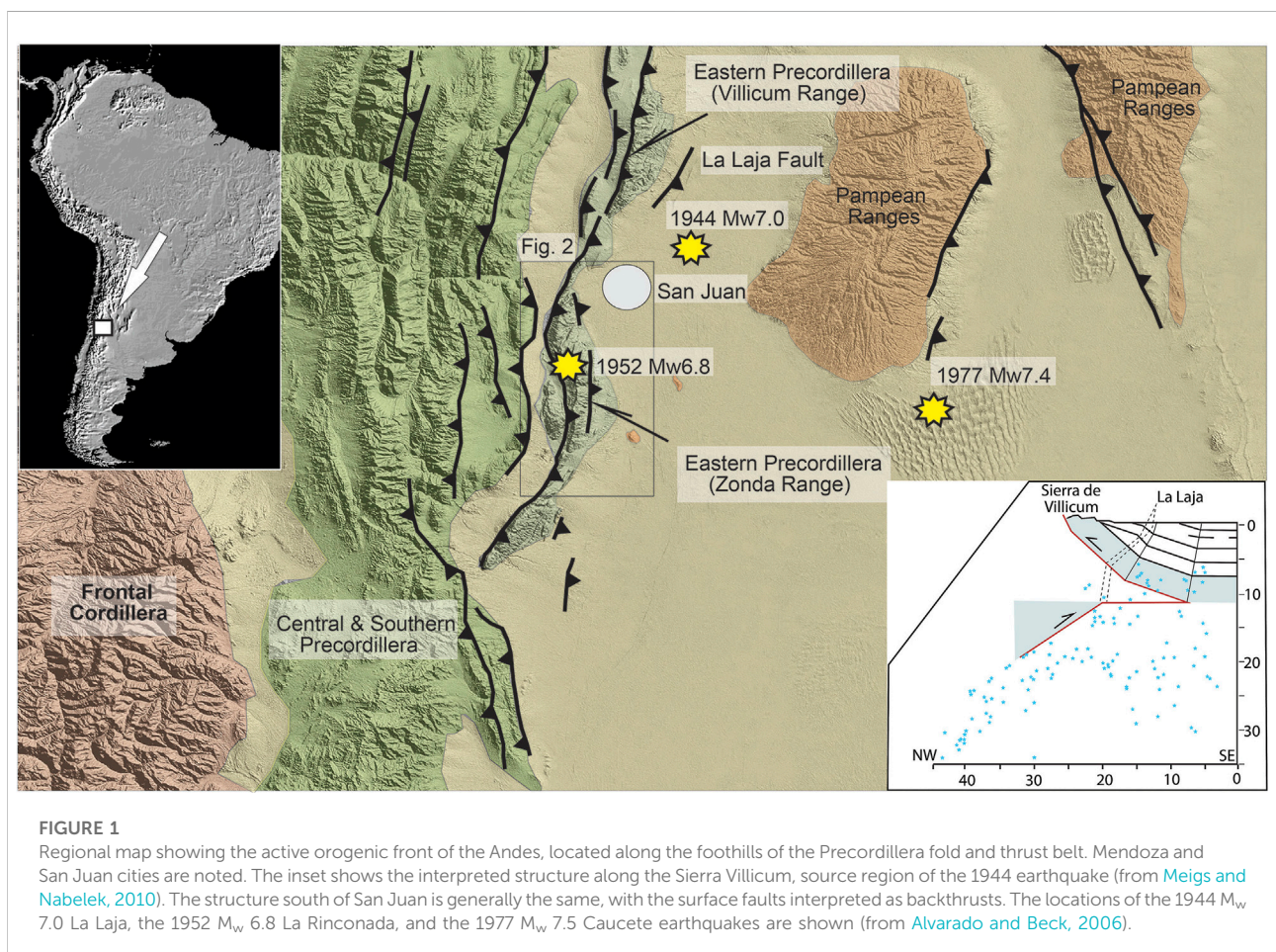
paleoseismology, San Juan earthquake hazard, Marquesado–La Rinconada fault, Eastern Precordillera, Argentina, Andes

Introduction

The retroarc thrust belt along the eastern flank of the Andes is one of the most potentially hazardous shallow crustal seismic zones in South America because of its high strain rate and active mountain-building (Brooks et al., 2011; Weiss et al., 2015; Costa et al., 2021). However, the blind nature of faulting along most parts of the Andean orogenic front and the vegetation cover over much of its length, aside from making it difficult to access, resulting in scarce exposure of the Quaternary deformation zones, hampering a suitable analysis of the paleoseismic record of these Quaternary thrusts (Dumont, 1996; Audemard, 1999; Baby et al., 1997; Bes de berc et al., 2005; Costa et al., 2021; Lombardo and Grützner, 2021, among others). In Central Western Argentina, the active faults expressed at the surface crop out along the east flank of the Eastern Precordillera (Bastías et al., 1984; Fielding and Jordan, 1988; Costa et al., 2006) (Figures 1, 2), where historical crustal earthquakes have severely damaged the Mendoza and San Juan urban areas. The Eastern Precordillera is a narrow belt of west-vergent surface thrusts between the east-vergent Precordillera fold-and-thrust belt to the west and the basement uplifts of the Sierras Pampeanas structural

province to the east (Figure 1) (Ortiz and Zambrano, 1981; Fielding and Jordan, 1988; von Gosen, 1992; Cristallini and Ramos, 2000). It has been proposed that active upper crustal deformation in the Eastern Precordillera is directly linked to structures in the middle and lower crust (Figure 1) (Ramos et al., 2002; Vergés et al., 2007; Meigs and Nabelek, 2010; Bellahsen et al., 2016). Thus, active faults and folds exposed throughout the Eastern Precordillera provide constraints on the rates and timing of crustal shortening and seismic hazards related to crustal faults (Costa et al., 2000, 2014, 2019; Ahumada and Costa, 2009; Schmidt et al., 2011; Rockwell et al., 2014; Richard et al., 2019; Rimando et al., 2019).

The 1944 M_w 7.0 La Laja and the 1952 M_w 6.8 La Rinconada earthquakes occurred beneath the eastern piedmont of the Eastern Precordillera of San Juan (Figure 1). However, many open questions remain regarding the nature and characteristics of the suspected earthquake sources. Whereas the 1944 event ruptured along discrete pre-existing scarps (Castellanos, 1944; Groeber, 1944; Instituto Nacional de Prevención Sísmica, 1982; Bastías et al., 1984; Paredes and Perucca, 2000; Meigs et al., 2006; Rockwell et al., 2014, among others), no records of surface deformation have been reported for the 1952 earthquake.



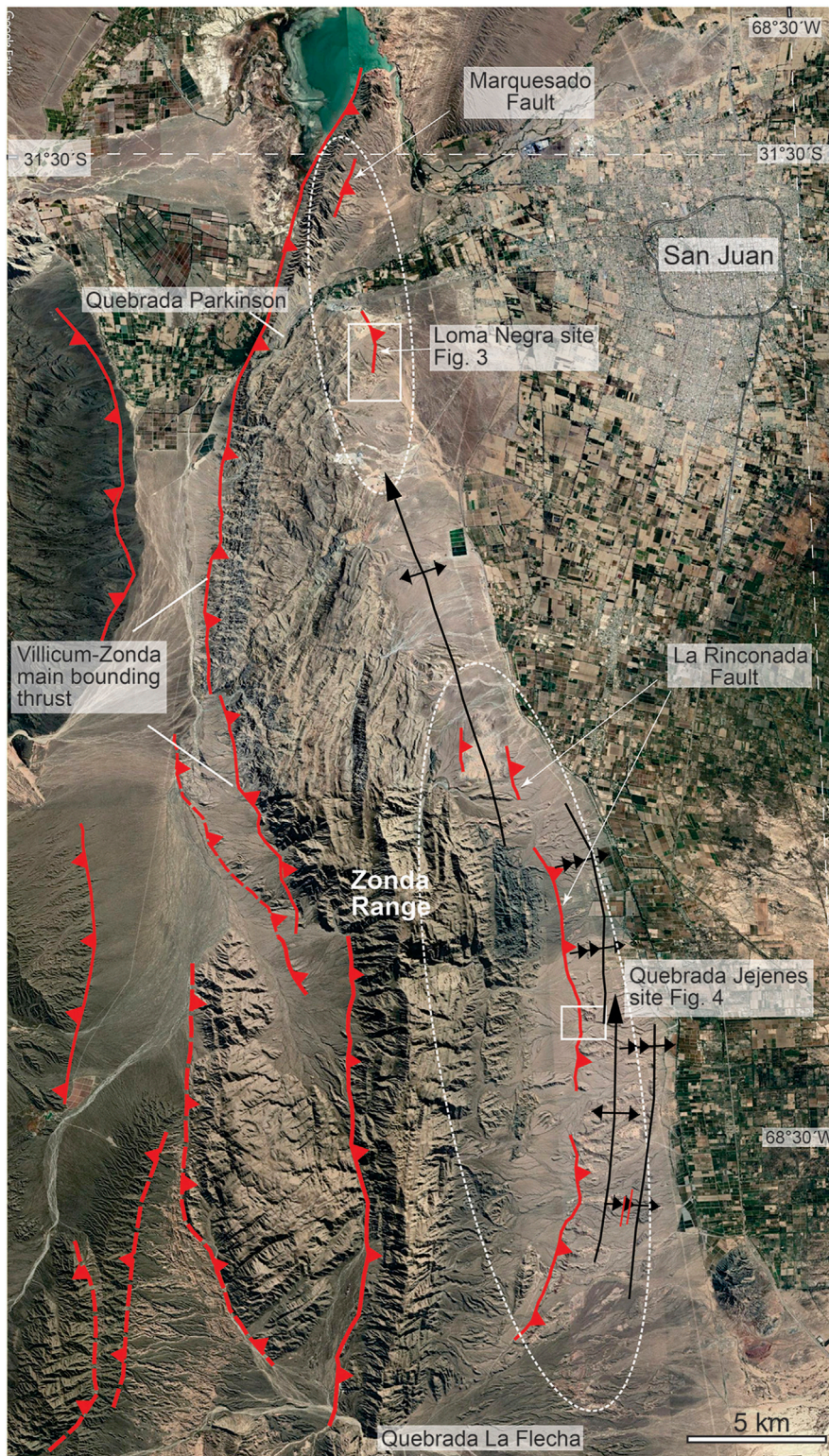


FIGURE 2

Google Earth image of the Eastern Precordillera along the Chica de Zonda range front. It should be noted that the west-verging faults produce uphill-facing scarps in the piedmont, interpreted as backthrusts that have emerged along bedding, resulting in areas of alluvial ponding. The areas where paleoseismic trenching were undertaken are indicated as the Loma Negra and Jejenes trench sites, with detailed maps presented in [Figures 3, 4](#).

Analyses of the historical seismograms of the 1944 hypocenter yield alternative depths for the event. Alvarado and Beck (2006) argue for a <12 km depth (Instituto Nacional de Prevención Sísmica, 1982). In contrast, Meigs and Nabelek (2010) place the event at ~25 km. The 17–30 km depth range of the 1977 Caucete and other, deeper events (Kadinsky-Cade, 1985; Alvarado et al., 2005), however, imply that active faults lying beneath the Eastern Precordillera and Sierras Pampeanas regions extend through the crust. Given that surface rupturing faults along the east flank of the Eastern Precordillera include both long-lived west-vergent thrusts and flexural-slip faults related to crustal-scale folds (Costa et al., 1999; Meigs et al., 2006; Rockwell et al., 2014), the rupture of the La Laja fault in 1944 underscores the challenge of linking coseismic surface ruptures with source faults at depth (Figure 1; Meigs et al., 2006; Vergés et al., 2007; Meigs and Nabelek, 2010).

Rockwell et al. (2014) addressed the deformation record of the La Laja fault near the epicentral area of the 1944 event for the past ~35 ka. They document nine surface-rupturing earthquakes with similar or even larger coseismic slip than occurred during the 1944 M_w 7.0 La Laja earthquake. Age data indicate an average recurrence interval of ~4 ka for events that rupture the La Laja fault.

Unveiling the earthquake history of the active faulting is a necessary effort given the hazard that these structures pose for the Mendoza–San Juan region (~2 million people). In this paper, we present the results of detailed mapping and trenching at two sites along the Marquesado–La Rinconada fault zone, the longest and most continuous fault with surface expression in the Eastern Precordillera (Groeber, 1944) (Figure 2). A pattern of meter-scale surface ruptures on faults with millennial-scale recurrence for the active fault of the Eastern Precordillera has emerged from these new data.

Regional tectonic setting

The Central Andes are generally regarded as a type-example of noncollisional fold-and-thrust belts (Jordan et al., 1983), where mountain building is principally driven by subduction geodynamics (Ramos, 1988, 2009; Gutscher et al., 2000; Oncken et al., 2006). The study area is in the South Central Andes, where the collision of the Juan Fernández aseismic ridge after ~8 Ma and consequent flat-slab subduction are the main events that have controlled the orogenesis between 27 and 33°S latitudes (Gutscher et al., 2000). The orogenic front on the east flank of the Andes migrated eastward with time, resulting in the successive growth of the Principal Cordillera, Frontal Cordillera, and Precordillera from west to east (Ramos, 1988, 2009; Ramos et al., 2002). Precordillera fold-and-thrust belt structures developed during the Pliocene and Pleistocene (Ramos, 1988). A shift of deformation from the Precordillera into the Eastern Precordillera and Sierras Pampeanas structural provinces is attributed to the onset of flat-slab subduction (Jordan et al.,

1983; Jordan and Allmendinger, 1986; Fielding and Jordan, 1988; Ramos et al., 2002). Crustal shortening across the east flank of the Andes absorbed ~60–75% of the total convergence between the trench and the foreland at 30°S over the past 10–15 Ma (Allmendinger et al., 1990).

The amount of seismic energy released in the upper plate along flat-slab segments is argued to be, on average, three to five times greater than in sectors with normal subduction angles (Gutscher et al., 2000). Accordingly, nearly 50% of the documented Quaternary deformation and the most active structures in Argentina are concentrated within the Andean Orogenic Front between 27 and 32° S latitudes (Costa et al., 2000; Costa et al., 2006; Costa et al., 2021; <https://sigam.segemar.gov.ar/visor/>). GPS-derived velocity fields support these results, which suggest elastic shortening rates between the Eastern Precordillera and the Western Sierras Pampeanas range from 2 to 7 mm/a (Kendrick et al., 1999; 2001; Brooks et al., 2003), coincident with large historical seismicity that is concentrated between the Precordillera and the Sierras Pampeanas (Cahill and Isacks, 1992; Smalley et al., 1993; Engdahl et al., 1998; Gutscher et al., 2000; Alvarado and Beck, 2006; Alvarado et al., 2009).

Structural geometry and style vary both across and along strike, which reflects the combined influences exerted by the Paleozoic sedimentary prism in the shallow crust and the reactivation of Paleozoic thrust structures in the middle and lower crust (Ramos, 1998; Ramos et al., 2002). Imbricate thrust slices in the east-vergent Precordillera formed above a décollement in Silurian strata (von Gosen, 1992). Exposures of Cambro-Ordovician sediments suggest a stratigraphically lower detachment in Cambrian rocks characterized by the west-vergent Eastern Precordillera upper crustal structures (Meigs et al., 2006; Vergés et al., 2007; Richard et al., 2019). Precambrian metamorphic rocks exposed at the surface, along with seismicity to depths of 40 km, indicating that the Sierras Pampeanas structures extend through the crust (Kadinsky-Cade, 1985; Smalley et al., 1993; Ramos and Vujovich, 2000; Ramos et al., 2002; Galindo et al., 2004).

The zone of current deformation corresponds to a N-S-trending belt of active faulting and folding, crustal seismicity, and interseismic strain accumulation that spans the Eastern Precordillera and Sierras Pampeanas structural provinces (Figure 1) (Instituto Nacional de Prevención Sísmica, 1982; Kadinsky-Cade, 1985; Smalley et al., 1993; Brooks et al., 2003; Alvarado and Beck, 2006; Meigs and Nabelek, 2010; Costa et al., 2021). The locus and partitioning of active thrusting change systematically along strike from north to south. At the latitude of San Juan (~31.5°S; Figure 1), fold and fault scarps in terraces, along with other evidence of active faulting, are restricted to the eastern flank of the Eastern Precordillera and the Sierras Pampeanas regions (Fielding and Jordan, 1988; Meigs et al., 2006; Vergés et al., 2007). The Precordilleran and Eastern Precordilleran frontal thrusts juxtapose Paleozoic rocks against Neogene redbeds, and offset terraces reveal that these range-

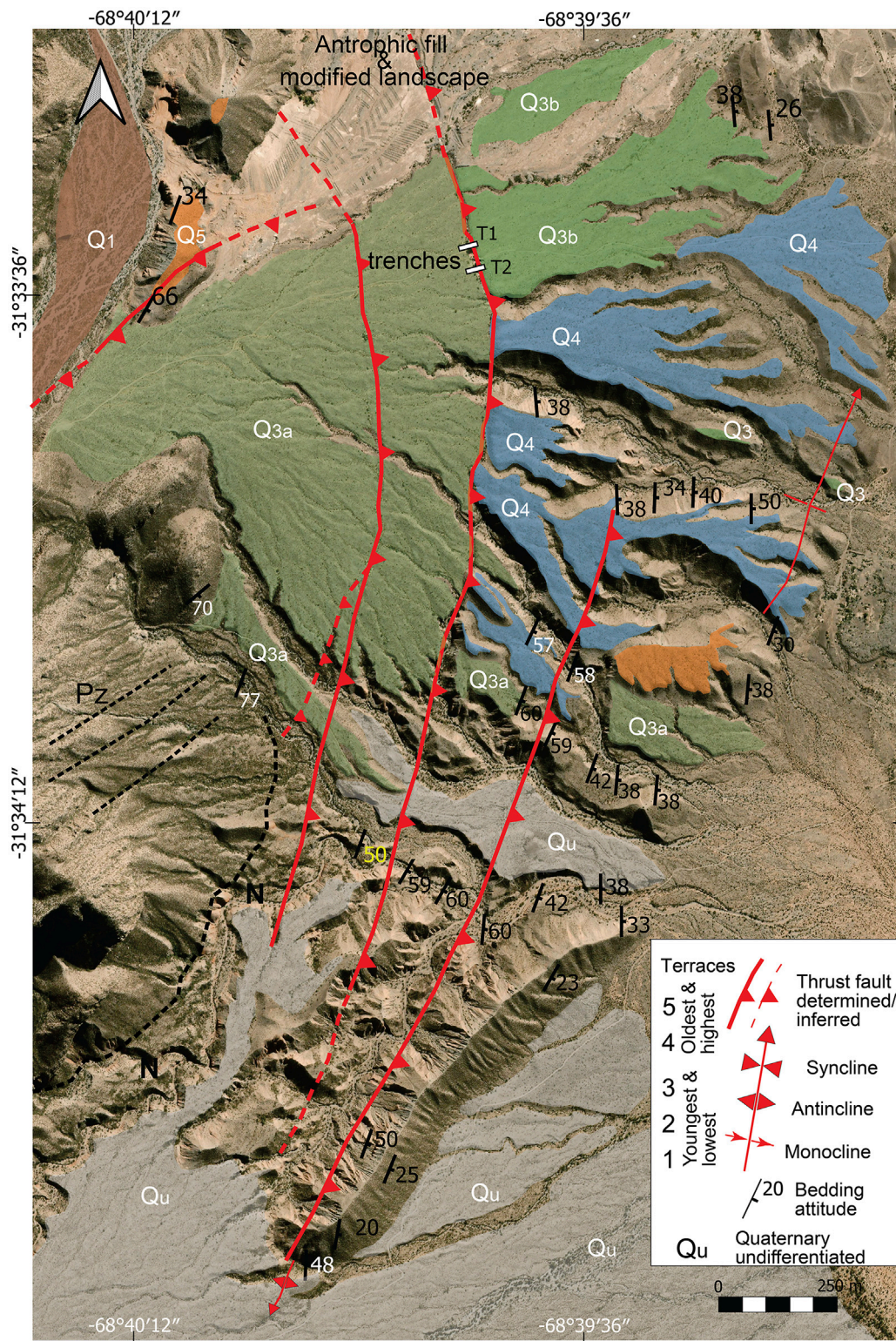
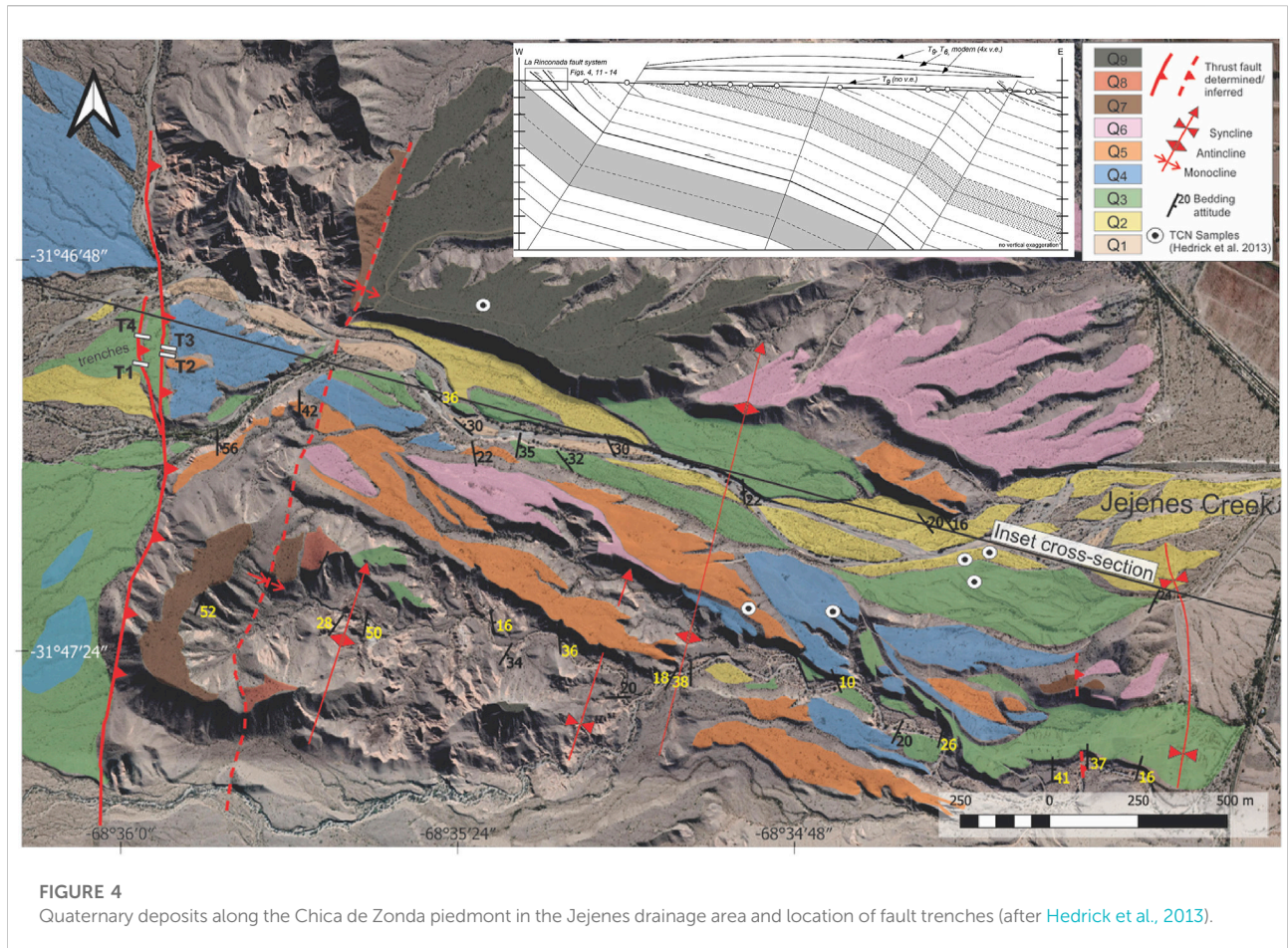


FIGURE 3 Quaternary alluvial deposits and underlying structure of the Miocene bedrock in the Loma Negra area. Locations of trenches 1 and 2 are indicated by small rectangles. It should be noted that the Q2 deposits of Hedrick et al. (2013) are remapped here as Q3a based on our new age data (revised from Hedrick et al. 2013).



bounding faults are active in the Quaternary in many cases (Paredes and Bastías, 1987; Uliarte et al., 1987; Siame et al., 2002; Ahumada and Costa, 2009; Perucca and Vargas, 2014; Blanc and Perucca, 2017). To the south, at ~ 32°S, active faulting is distributed between west-dipping faults that mark the Southern Precordillera thrust front (Las Peñas and Las Higueras thrusts) and east-dipping thrust sheets comprising the Eastern Precordillera (Costa et al., 2000; Vergés et al., 2007; Ahumada and Costa, 2009; Costa et al., 2014). Nominal amounts of shortening at low rates characterize the Pampean ranges, located ~250 km to the east (Costa et al., 2018; Costa et al., 2021).

Methods

We mapped bedrock, alluvial fans, and river terraces in each of the two study sites using Google Earth imagery and aerial photography (Figures 3, 4). A site-specific river terrace and alluvial fan nomenclature were adopted for the two study sites. The relatively youngest surface, typically an active channel or fan, was denoted by the symbol Q1, and

topographically higher surfaces were indicated by successively higher numbers. The number of surfaces and relative age nomenclature are not directly correlative between the two study sites. The correlation of surfaces between sites relied on absolute surface exposure dates. Terrestrial cosmogenic nuclide (TCN) surface exposure and burial ages and optically stimulated luminescence (OSL) ages have been reported for both study areas by Hedrick et al. (2013). New OSL and ¹⁴C ages presented in this paper provide additional control for the younger deposits and surfaces.

Faults expressed at the surface typically verge west, uphill relative to the eastward sloping terrace and alluvial fan surfaces that flank the Eastern Precordilleran ranges. Uphill-facing fault scarps, against which fine-grained alluvium and scarp erosional products accumulate, provide nearly ideal sites to excavate paleoseismic trenches (Rockwell et al., 2014). These areas pond and trap sediment on the surface of the terrace in the fault footwall. Material that accumulates above the terrace deposit includes fine sand and silt transported between faulting events and colluvial material produced by scarp degradation immediately after an event. We excavated two trenches at the Loma Negra site on the Marquesado fault and

four trenches at the Quebrada Jejenes site on the La Rinconada fault to constrain the rupture history of the Marquesado–La Rinconada fault system (Figure 2).

The trenches were excavated to a depth of ~2.5–3 m, with steeply sloping walls to ensure stability. Each trench face was photographed meter by meter, from which we constructed photomosaics for most trench walls, except for Jejenes T1. Logging was accomplished on print-outs of the photomosaics at a scale of about 1:10; Jejenes trench T1 was logged on graph paper. The sediment characteristics were described at each site (Supplementary Material). OSL and charcoal samples were collected to provide age control for the faulted units. For the Loma Negra trench site, we also dug soil pits upslope and downslope from the trenches (Figure 3) to establish whether the alluvial fan surfaces correlate across the fault; soils were described according to Soil Survey Staff (1993; updated to 2017).

The OSL samples were collected by driving opaque black tubes (ABS) into the finer-grained silty sand strata, covering the tubes in aluminum foil, and then taping and preparing them for transport to the laboratory. The OSL samples were processed at the Luminescence Laboratory at the University of Cincinnati following standard published procedures (Supplementary Text). The charcoal samples were collected in glass vials and transported back to the Quaternary Laboratory at SDSU. They were cleaned and picked under a microscope before processing for AMS ^{14}C dating at the UCI CAMS facility, and all ages were calibrated using OxCal v4.4.4 (Bronk-Ramsey, 2021; atmospheric data from Reimer et al., 2020).

Structural setting of active faults on the eastern flank of the Eastern Precordillera

The Marquesado and La Rinconada fault zones crop out along the eastern piedmont and backlimb of the Sierra Chica de Zonda, one of the west-vergent thrust sheets that constitute the Eastern Precordillera (Figure 1) (Ortiz and Zambrano, 1981). As is typical in the Eastern Precordillera, a discontinuous series of faults and fold scarps mark the surface expression of active deformation. Active folds and faults crop out along the length of Sierra Chica de Zonda, which extends more than 50 km to the south of the San Juan River (Figure 2; Groeber, 1944; Bastías et al., 1984; Martos, 1987; Costa et al., 1999; Richard et al., 2019; Rimando et al., 2019, among others). Faults tend to have moderate-to-steep dips and have the same dip as bedding in the Neogene bedrock. Whereas some faults cut bedding, the fact that most faults are bedding-parallel supports the interpretation of the faults as either backthrusts with a hanging wall flat geometry or as flexural-slip faults related to folding (Costa et al., 1999; Meigs et al., 2006; Rockwell et al., 2014). The observation that active surface faulting south of San Juan is confined to a single thrust fault zone better supports the

backthrust hypothesis, as flexural-slip faulting should be volumetric and occur over a broad width of the folded rocks.

The trenches provide evidence for multiple Late Quaternary faulting events at each site, which constrain the timing of past large earthquakes. The stratigraphic packages exposed by the trenches at each location were generally similar. A coarse alluvial fan or terrace deposit unconformably overlies Neogene bedrock, which is overlain in turn by alternating ponded alluvial and colluvial deposits. We first present results from the Loma Negra site along the Marquesado fault in the north and then the Quebrada Jejenes site, located along the La Rinconada fault in the south. The results from each site are compared to one another and other studies along the eastern flank of the Eastern Precordillera in the Discussion section.

Loma Negra site, Marquesado fault

The Loma Negra site lies near the northern end of the Sierra Chica de Zonda and comprises a set of <2 km-long fault segments that discontinuously crop out from Embalse de Ullum (31.46°S, 68.65°W) to an unnamed dry riverbed ~20 km to the south (31.65°S, 68.65°W). The northernmost and longest fault in this part of the fault system strikes sub-parallel to the NE trend of the Zonda thrust, which bounds the west flank of the range (Figure 2). A clearly defined, linear ~2 km-long scarp characterizes the fault trace, which lies between the Rio San Juan and Quebrada de Zonda to the south, a paleochannel of the Rio San Juan. The fault developed within homoclinal Cenozoic redbeds, which dip 24° to 35°E, thrust over the thin and tabular Quaternary alluvium that unconformably overlies bedrock (Instituto Nacional de Prevención Sísmica, 1982; Paredes and Bastías, 1987; Costa et al., 2000; Perucca and Vargas, 2014), and has been imaged by geophysical methods (Correa-Otto et al., 2018).

Three subparallel, <1 km long faults and a fold scarp comprise the Marquesado fault system at Loma Negra (Figure 3). A curved map trace and east dip that mimics the strike of bedding in the Neogene bedrock defines the fault topology (Figure 2). Fault strike is discordant, however, to the NE–SW-trending bedding of the Paleozoic rocks, suggesting that Cenozoic bedding surfaces control the orientation of the fault planes. We trenched two of the three fault strands at the Loma Negra site, although only the central strand accumulated fine-grained alluvium that could be interpreted and dated.

Loma Negra trenches

Two trenches (T1 and T2), spaced about 10 m apart, were excavated in a closed depression containing ponded alluvium on the middle of the three fault strands at Loma Negra (Figure 3). The stratigraphic section in each trench was nearly identical and

is summarized in the [Supplementary Material](#). Units 400–600 were coarse, sandy gravel alluvium interpreted as alluvial fan deposits. Unit 600 in the hanging wall was interpreted to be older than unit 400 in the footwall because the soil developed in unit 600 was better developed than in unit 400 upslope from the trench (soil descriptions in [Supplementary Material](#)). All deposits younger than unit 400 in the footwall were finer-grained and interpreted as deposits that accumulated against the uphill-facing scarp created by hanging wall uplift and folding. Some of the fine-grained ponded alluvium may have resulted from dust production from rockfalls produced by earthquakes (Rockwell et al., 2014; Karlsson et al., 2021). Although some of the dust may have been derived from nearby playas, most deposition at the scarp is likely the consequence of channeled flow on the alluvial fan surface transporting fines toward the fault scarp. Strata in the hanging wall, composed entirely of massively bedded sandy gravel, warps down to the west into the fault. We interpreted this as a hanging wall fault-related fold.

Five faulting events were interpreted from the Loma Negra trenches, which we named E1 (most recent) to E5. Event E5, indicated by a purple contact in [Figures 5, 6](#), is interpreted to have displaced units up through 300 and produced a colluvial wedge of clastic material, indicated as CW5 in [Figures 5, 6](#). Unit 300 is the most recent evidence of the transport and deposition of gravel on this part of the alluvial fan. Event 5 forced deposition of CW5 and units 290 and 280, which thicken against the fault scarp. A discrete colluvial wedge is best identified in trench T1S (CW5; [Figure 5B](#)), where it buries unit 300 and is overlain by unit 280. An older fine-grained fill, unit 350, is present in the fault zone and may indicate an earlier event, but no other observations support this, as the trenches were not deep enough. In T1N ([Figure 5A](#)), unit 280 is wedge-shaped, thickening toward the fault, and is interpreted as age-equivalent or younger than CW5. Although CW5 ought to have consisted primarily of coarse gravelly alluvium derived from the hanging wall, CW5 is composed primarily of fine-grained silty sediment in the footwall. [Figure 6](#) shows a possible section of CW5 between fault strands, which may explain the finer grain size in the footwall of the lower strand. The lithology of units 280 and 290 suggests that silty sediments may get blown up against the scarp and represent the primary source of colluvial material in some exposures. In trench T2, a possible colluvial wedge associated with E5 is present on both walls ([Figure 6](#)), but it is re-faulted in the T2N exposure and now resides in the hanging wall of the lowest fault. Notably, the possible CW5 colluvial wedge is matrix-supported gravel, which contrasts with the grain-supported units 300 and 400, supporting the colluvial wedge interpretation. Additional evidence for event E5 in T1N and T1S is the presence of ponded alluvial strata of units 290 and 280, which demonstrate that a scarp was present in the pond alluvium. OSL data indicate that unit 350 is 17.8 ± 4.4 ka, CW 5 is $14.9 \pm$

3.2 ka, and unit 290 is 14.6 ± 1.7 ka, constraining the approximate age of event E5 to between 15 and 18 ka.

Event E4, indicated by the green horizon in [Figures 5, 6](#), is interpreted to affect units 280 and older. In trench T1S, a fault splay breaks up through unit 280 and is capped by unit 270. In trench T2N, a fault splay breaks up into unit 280 but is disrupted by a filled burrow; this strand is also capped by unit 270. In all trench exposures, unit 270 itself is wedge-shaped (CW4?) with a gravelly basal wedge capped by finer colluvium, consistent with colluvial growth from the scarp. However, the fine-grained component does not have an obvious source. Either silty material blew up against the scarp or most of the colluvium was derived from a fine-grained surface soil on the hanging wall, which suggests that the thrust tip may not have reached the surface locally. Unit 270 yielded an OSL age of 15.3 ± 4.7 ka ([Figure 6A](#)).

Event E3, indicated by the orange horizon in [Figures 5, 6](#), is interpreted to have occurred after the deposition of unit 230 and before the deposition of the wedge-shaped unit 220 (CW3). A fault splay cuts up through unit 230 and is capped by unit 220 in T1N ([Figure 5B](#)) and possibly in T2N ([Figure 6A](#)). The geometry of unit 220 suggests that it is a colluvial wedge. The lithology of unit 220 is almost entirely fine-grained, which implies that a relatively thick mantle of fine-grained material coated part of the scarp to source the fine-grained wedge. A small clastic deposit interfingers with the fine-grained wedge exposed in T2S and T1S, and fine-grained wedges are present in the footwall of a secondary fault splay in T2S and T1S. Whereas the fine-grained wedges may not be classic colluvial wedges that result from the gravitational collapse of the coarse hanging wall gravel, stratigraphic relationships and geometries are consistent with a coseismic or immediate post-seismic origin and imply that fine-grained sediments were blown up against the scarp and were the surface deposits on the scarp at the time of this event. Unit 230 had an OSL age of 8.7 ± 1.0 ka. Unit 260 yielded OSL ages of 12.4 ± 3.4 ka ([Figure 5A](#)), 15.3 ± 1.8 ka ([Figure 5B](#)), and 17.2 ± 2.7 ka ([Figure 6](#)).

Event E2, represented by the yellow horizon in [Figures 5, 6](#), is interpreted as a fault rupture that deformed sediment up through or within unit 135 and is capped by unit 130. In trench face T1N, a small wedge of clastic colluvium is interpreted as a colluvial wedge (CW2), although the relationship is not clear because of later faulting that transferred CW2 to the footwall. In trench faces T1S and T2S, fault splays appear to cut up through unit 140 and are capped by unit 130. In T2N, unit 135 seems to be folded and to be capped by unit 130, and it is not clear whether 135a is faulted or is colluvium that post-dates the event. OSL samples yielded ages of 12.9 ± 2.4 ka for unit 200 and 7.4 ± 1.2 ka for unit 160, whereas samples from unit 135 yielded ages of 9.1 ± 1.5 ka, 9.3 ± 1.9 ka, and 13.2 ± 2.5 ka.

The youngest event, E1, indicated by the blue horizon in [Figures 5, 6](#), was suggested by a fault splay that breaks unit 130 in T1S and is capped by unit 100, a clastic stratum shed from the

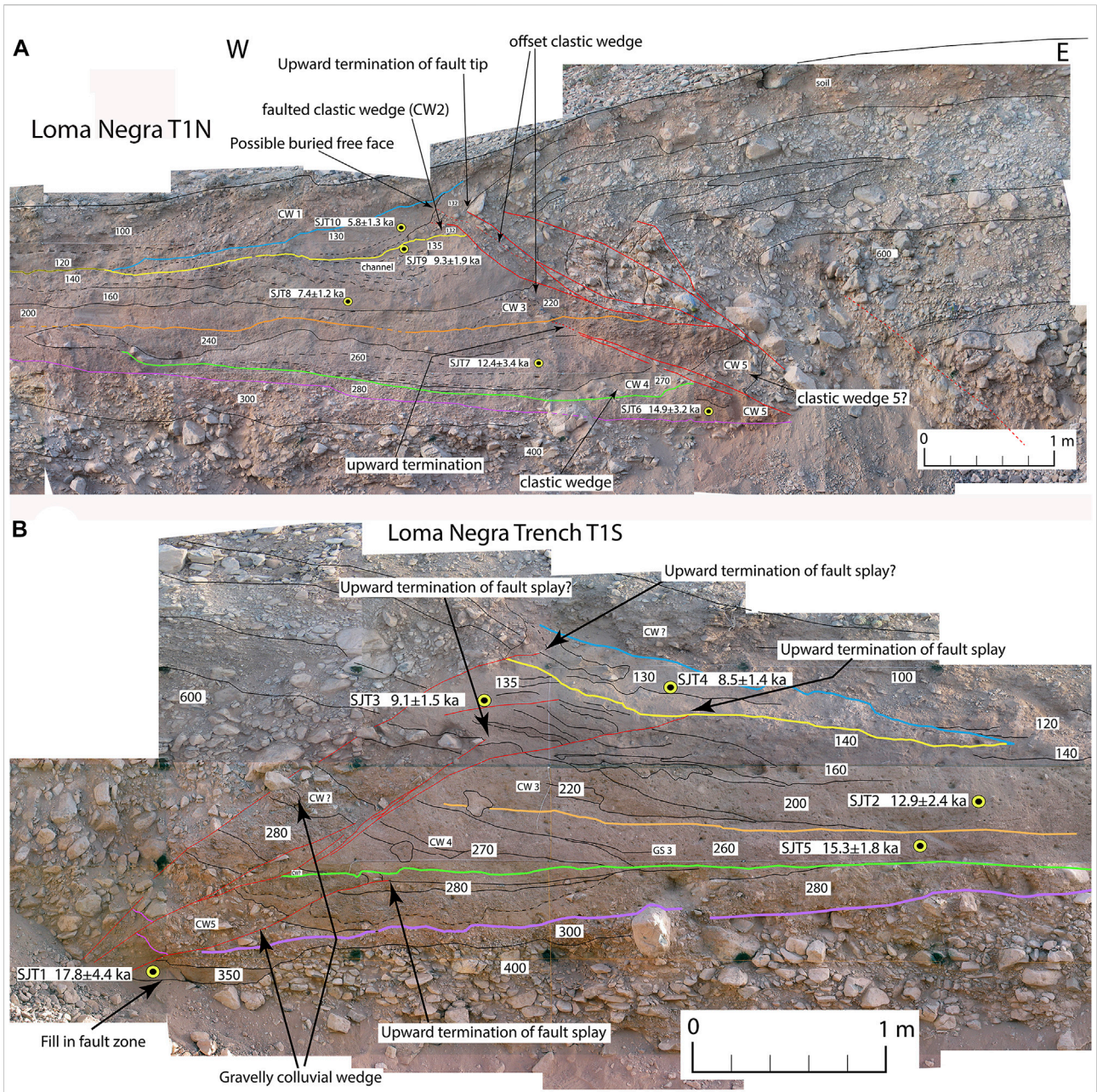


FIGURE 5
(A) Log of the north wall of Loma Negra trench T1 (T1N). CW indicates the position of interpreted colluvial wedges based on their wedge-shaped geometry and truncation against the fault. Colored lines indicate the ground surface at the timing of each event, as discussed in the text. Sample locations are tied to the OSL dating presented in [Table 2](#). **(B)** Log of the south face of Loma Negra trench T1 (T1S). CW indicates the position of interpreted colluvial wedges based on their wedge-shaped geometry and truncation against the fault. Colored lines indicate the ground surface at the timing of each event, as discussed in the text. Sample locations are tied to the OSL dating presented in [Table 2](#).

hanging wall. In T2S, the E2 event horizon (yellow contact) and unit 130 above appear tilted and unconformably overlain by unit 100 ([Figure 5B](#)). A fault splay cuts the yellow contact and extends upward into unit 130. Unit 100 above the blue contact appears to have a monoclinical form, which suggests that either the base of unit 100 is folded or that unit 100 was deposited across a fold

scarp ([Figure 5B](#)). In trench face T1N, the blue contact appears rotated, but the tilt is ambiguous. In T2N, the blue contact is not readily visible and thus yields equivocal evidence for deformation, although clastic unit 100 caps all faults and older strata. These observations suggest that event E1 had relatively minor surface effects when compared to the older interpreted

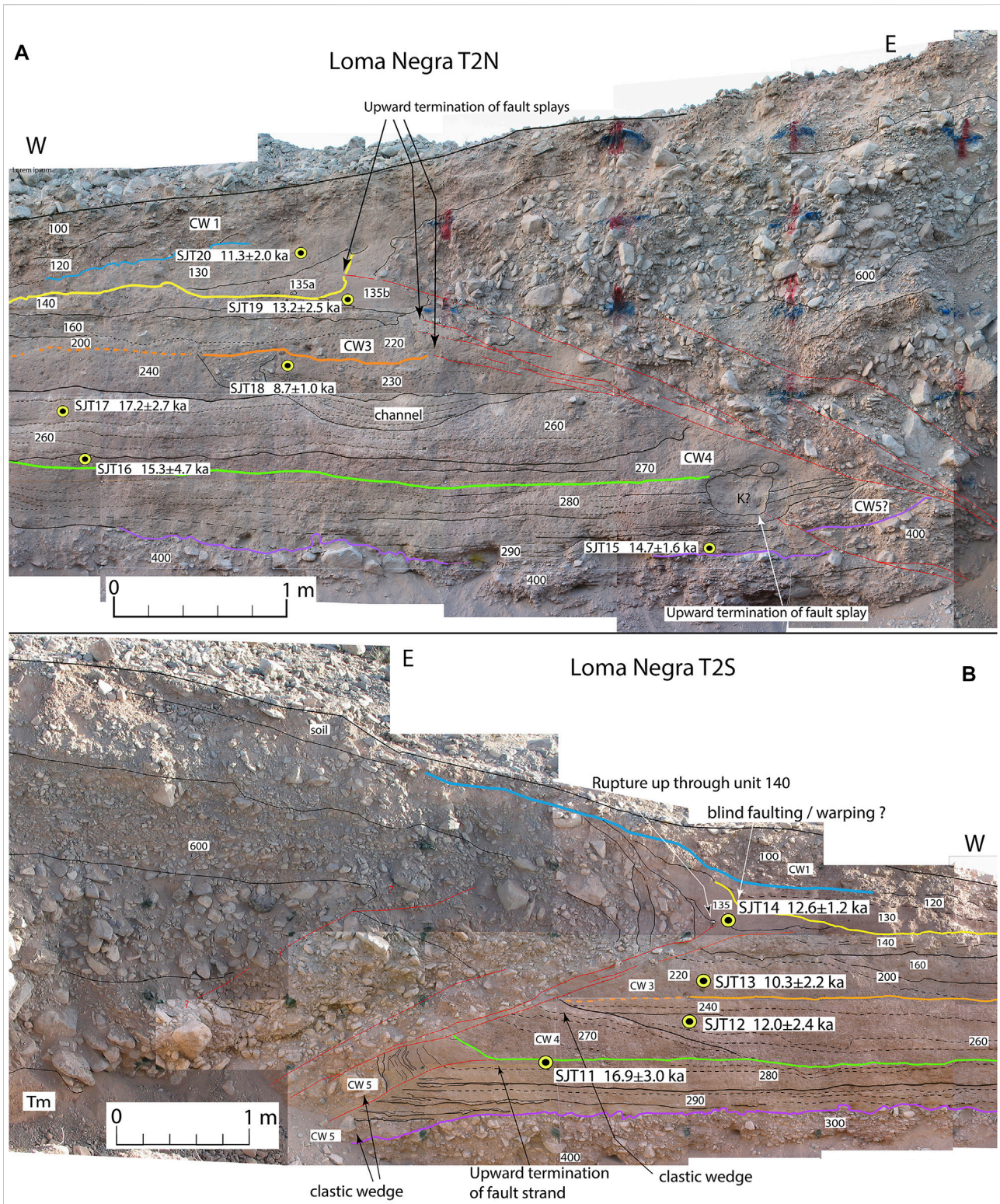


FIGURE 6

(A) Log of the north face of Loma Negra trench T2 (T2N). CW indicates the position of interpreted colluvial wedges based on their wedge-shaped geometry and truncation against the fault. Colored lines indicate the ground surface at the timing of each event, as discussed in the text. Sample locations are tied to the OSL dating presented in Table 2. (B) Log of the south face of Loma Negra trench T2 (T2S). CW indicates the position of interpreted colluvial wedges based on their wedge-shaped geometry and truncation against the fault. Colored lines indicate the ground surface at the timing of each event, as discussed in the text. Sample locations are tied to the OSL dating presented in Table 2.

events. OSL ages for unit 130 are 13.2 ± 2.5 ka, 8.5 ± 1.4 ka, and 5.8 ± 1.3 ka.

Altogether, we recognize stratigraphic evidence for up to five surface-rupturing (or near surface-rupturing) events that post-date deposition of units 300 and 400 (which are the same deposit in some exposures). Collectively, reconstruction of the top of unit 300 with the Q3 alluvial fan surface east of the fault requires a maximum of 10–12 m of dip displacement on a 30–40° dipping fault based on estimates from T2; this dip is consistent with Neogene bedrock which dips 25°–38°E in the hanging wall near the trench (Figure 3). This slip estimate assumes that the scarp had been completely buried, which is unlikely, as the soil developed on the fan surface east of the fault precludes post-unit 600 deposition. The minimum dip displacement is indicated by the amount of slip required to place the hanging wall over unit 300/400, which is about 4 m in T1 and 5 m in T2. However, it is likely that units 300 and 400 accumulated against a scarp, as they are interpreted as younger than unit 600 based on soil development. The minimum estimate assumes no erosion from the hanging wall, which is unlikely. If correct, this indicates that part of the 10–12 m implied by relief of the fan across the scarp also accrued during events that are older than unit 400. In any case, we estimate that dip displacement in the last five earthquakes, which post-dates deposition of the Q3 fan deposits, is between 5 and 12 m. This suggests an average minimum displacement per event of about 1 meter. The observation that most of the wedge-like colluvial deposits are fine-grained indicates that only minor amounts of coarse-grained alluvium were eroded from the hanging wall, suggesting that the minimum-slip estimate is close to the actual displacement.

Ages of interpreted Marquesado fault surface ruptures

We analyzed 20 OSL samples collected from units 130 down to 350 from the Loma Negra trenches (Table 1). Five of the samples (SJT2, SJT14, SJT17, SJT19, and SJT20) yielded ages that are greater than the underlying dates by more than their uncertainties. The dose rate was similar for all samples, as was the water content, as expected for an arid environment, so the age inversions are not likely a result of variations in those parameters. Consequently, we interpret those five samples to have a partial bleach signal. The other 15 ages in Table 1 were placed into OxCal, along with the position of the event horizons, to calculate the event probability distributions (PDFs) for the interpreted earthquakes. Multiple ages from the same unit were analyzed as phases. Figure 7 shows the interpreted event ages for the past five surface ruptures. It should be noted that we did not date any samples from unit 100, so we cannot constrain the timing of the most recent event, which could, therefore, be as young as historical in age. The Oxcal model is presented in the Supplementary Material. The ages of the interpreted events

are E1 at 2.8 ± 2.8 ka, E2 at 7.1 ± 1.5 ka, E3 at 9.6 ± 1.3 ka, E4 at 14.4 ± 2.1 ka, and E5 at 17.2 ± 3.1 ka.

Quebrada Jejenes trench site, La Rinconada fault

The La Rinconada fault lies within a zone of folding and faulting that is ~25 km long and extends along the eastern flank of Sierra Chica de Zonda from an unnamed wash at ~31.67°S, 68.62°W southward to Quebrada La Flecha (31.91°S, 68.66°W; Figure 2). The La Rinconada fault system south of the Quebrada de Zonda lies ~2.5 km to the east and does not connect with the Marquesado fault to the north of the quebrada. La Rinconada fault has a nearly continuous trace characterized by a curvilinear (arcuate) geometry, a north trend, and an east dip (Groeber, 1944). Neogene redbeds that unconformably overlie Cambrian to Carboniferous limestones and clastic rocks in the Sierra Chica de Zonda crop out in the hanging wall of the fault (Bastías et al., 1984; Martos, 1987; Richard et al., 2019). The dip of the La Rinconada fault ranges from 29° to 50°E, parallel to the Neogene bedrock layering (Figure 4) (Bastías et al., 1984; Martos, 1987; Costa, 2009; Richard et al., 2019; Rimando et al., 2019). Scarp heights vary from 1 m in low, young river terraces to ~40 m across higher, older surfaces (Martos, 1987; Richard et al., 2019). Rimando et al. (2019) estimated a late Pleistocene shortening rate of 0.41 ± 0.01 mm/a for the La Rinconada fault, about half of the rate calculated for the La Laja fault north of San Juan (Rockwell et al., 2014).

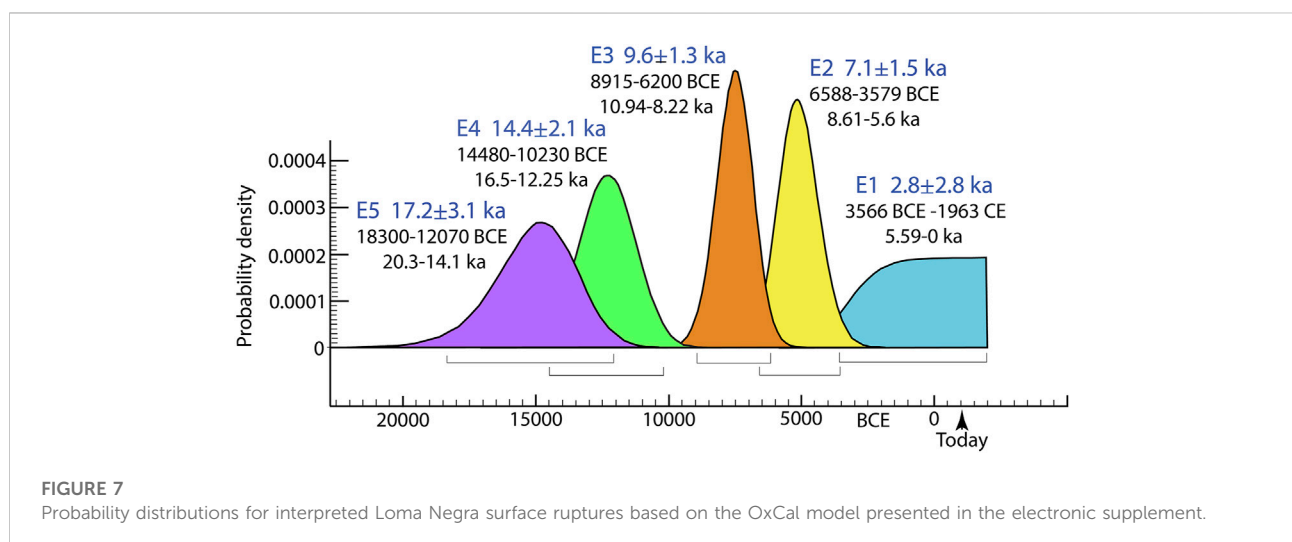
The La Rinconada fault at Quebrada Jejenes marks the western side of a ~3-km-wide region of folding, faulting, and uplift (Figure 4). A suite of nine fluvial terraces marked by 1–3 m thick gravel caps rest on a strath surface beveled into Neogene bedrock. The local relative age nomenclature of the geomorphic surfaces spans Q1 (youngest) to Q9 (oldest). Neogene bedrock defines an east-facing monocline (Figure 4). A broad, open fold across the monocline warps the terraces. Two splays mark the main western strand of the La Rinconada fault zone where it crosses the Quebrada Jejenes. The fault zone cuts terraces as young as Q2. The La Rinconada fault is interpreted as being parallel to the hanging wall and footwall bedding, as constrained by field and trench observations (Figure 4). An east-facing fold scarp expressed in all terraces and coincident with a decrease in Neogene bedrock dip from ~40° to 20°, from west to east, respectively, marks the eastern edge of the uplifted region.

Trenches at Quebrada Jejenes

Four trenches were excavated across the two closely spaced fault strands at the Quebrada Jejenes site (Figure 4). The fault strands are inferred to merge at shallow depths and should therefore record a similar earthquake history. Trenches

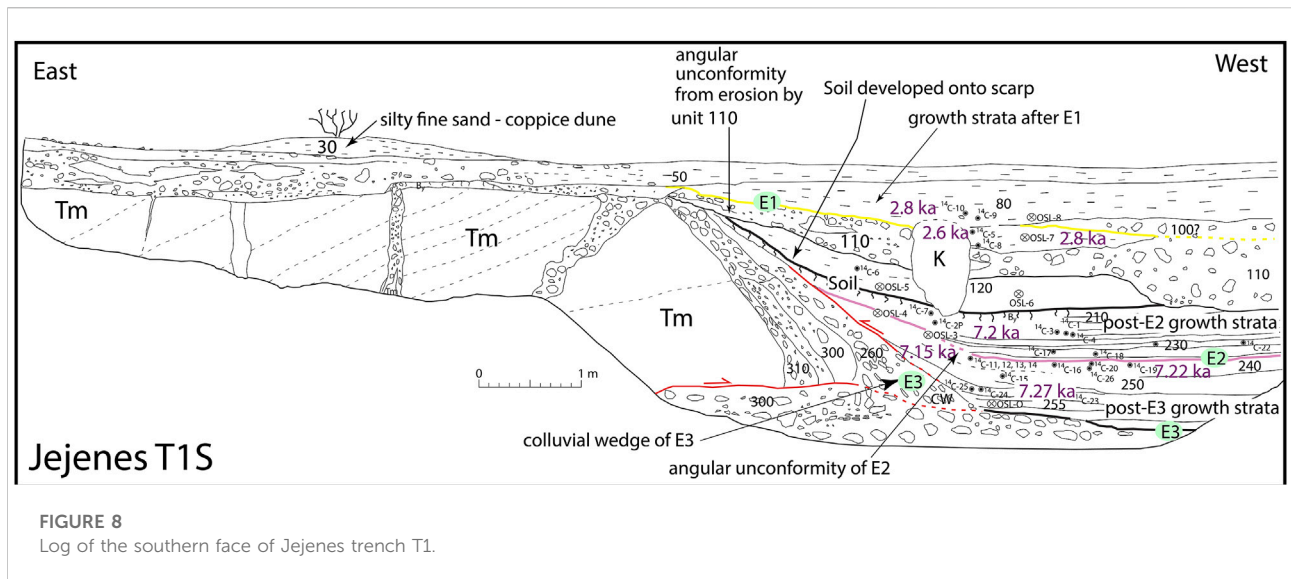
TABLE 1 Loma Negra OSL ages by unit. See the electronic supplement for the complete tables of OSL data. Italicized ages are out of stratigraphic order and were not used in the age model.

Unit	Trench	Sample #	OSL age	Comment
Event E1				
130	T1N	SJT10	5.8 ± 1.3 ka	Youngest OSL date
130	T1S	SJT4	8.5 ± 1.4 ka	
<i>130</i>	<i>T2N</i>	<i>SJT20</i>	<i>11.3 ± 2.0 ka</i>	<i>Out of stratigraphic sequence</i>
Event E2				
135	T1N	SJT9	9.3 ± 1.9 ka	
<i>135</i>	<i>T2S</i>	<i>SJT14</i>	<i>12.6 ± 1.2 ka</i>	<i>Out of stratigraphic sequence</i>
<i>135b</i>	<i>T2N</i>	<i>SJT19</i>	<i>13.2 ± 2.5 ka</i>	<i>Out of stratigraphic sequence</i>
140	T1S	SJT3	9.1 ± 1.5 ka	
160	T1N	SJT8	7.4 ± 1.2 ka	
<i>200</i>	<i>T1S</i>	<i>SJT2</i>	<i>12.9 ± 2.4 ka</i>	<i>Out of stratigraphic sequence</i>
220	T2S	SJT13	10.3 ± 2.2 ka	
Event E3				
230	T2N	SJT18	8.7 ± 1.0 ka	In the channel between 220 and 240
240	T2S	SJT12	12.0 ± 2.4 ka	From the base of the unit
260	T1N	SJT7	12.4 ± 3.4 ka	
260	T1S	SJT5	15.3 ± 1.8 ka	
260	T2N	<i>SJT17</i>	<i>17.2 ± 2.7 ka</i>	<i>Out of stratigraphic sequence</i>
270	T2N	SJT16	15.3 ± 4.7 ka	From the top of the unit
Event E4				
280	T2S	SJT11	16.9 ± 3.0 ka	From the top of the unit
280	T1N	SJT6	14.9 ± 3.2 ka	
280	T2N	SJT15	14.7 ± 1.6 ka	
Event E5				
350	T1S	SJT1	17.8 ± 4.4 ka	



T1 and T4 were located across the western strand, which is expressed as a scarp in the Q3 surface (Figure 4). The other two trenches (T2 and T3) were located about 40 m apart across the

eastern strand, which is marked by a scarp with Q3 in the footwall and Q4 in the hanging wall. The stratigraphic section was generally similar in trenches T1, T2, and T3 (Figures 8–10),



which is summarized in the [Supplementary Material](#). Trench T4 was not logged because the scarp did not trap much alluvium, and the stratigraphy was not adequate to interpret paleoseismic events.

Trench T1 was sited in a small drainage where alluvium was deposited across the projection of the fault scarp, with Q3 alluvium buried in the footwall (unit 300). Trenches T2 and T3 exposed sediment deposited on the Q3 surface in the footwall (unit 300) and were sited where alluvium was ponded against the scarp. The correlation of units between T1 and T2/T3 overlying unit 300 is uncertain, although the fluvial deposits of unit 300 provide some level of certainty that the general correlations are correct. For instance, units 100 and 110 are interpreted as fluvial in origin, which indicates that the scarp along the western fault strand was breached or completely buried.

Trench T1 was excavated in a drainage channel that incises into the Q3 alluvial fan deposited across the western fault strand ([Figure 4](#)). At the trench itself, the youngest stratum (unit 50) is undeformed channel alluvium in a small rill cut across folded Tertiary bedrock in the hanging wall ([Figure 8](#)). The Q3 alluvium (unit 300) unconformable contact with the Neogene bedrock (Tm) is exposed in the hanging wall, but the young channel alluvium of unit 50 has removed unit 300 (T3 surface) at the crest of the hanging wall fold. Unit 300 in the footwall section is overlain by interbedded fine-grained ponded alluvium and channel deposits (units 260 up through 80). Some of the fine-grained ponded alluvium likely represents reworked dust generated by rockfalls during the earthquake. Alternatively, the fine-grained ponded alluvium could entirely be sheet wash deposits or fine-grained lags accumulated following coarse-grained fluvial deposition. In any case, these strata accumulated against the scarp and are therefore growth strata.

Trenches T2 and T3 were excavated across the eastern fault strand. The footwall block exposes the Q3 alluvium at the base of the trench as units 300 and 310, whereas the hanging wall block is capped by unit 100 in T2N and Q4 alluvium in T2S and T3N ([Figures 4, 9, 10](#)). The T2 trench was sited to expose alluvium from a small, defeated drainage warped up across a 40-cm-high scarp at the fault, which is observed in the north face of trench T2 ([Figure 9A](#)). This low scarp likely preserves evidence of the youngest event.

Evidence for four faulting events is exposed in the trenches across the eastern strand, whereas only three events are interpreted from T1 across the western strand. We only have age data from the trench exposures to constrain the timing of the three most recent events. The oldest event age is constrained by the ^{10}Be cosmogenic exposure data for Q3 described as follows ([Hedrick et al., 2013](#)).

Evidence for the oldest rupture, event E4, is best expressed in the T2S and T3N exposures where unit 270 contains substantial matrix material and is interpreted as fault-generated colluvium produced by E4. As unit 270 buries unit 300, interpreted as the Q3 surface deposits, E4 must post-date deposition of Q3 alluvium. Evidence for this event is the weakest among the four interpreted ruptures.

Several observations reflect the occurrence of event E3. Bedrock is thrust over the interpreted colluvial wedge of unit 270, with the thrust tip overlain by unit 260, as revealed in trenches T1S, T2S, and T3N ([Figures 8, 9B, 10](#)). An angular unconformity marks the upper contact of unit 260 and younger deposits. The coarse, wedge-shaped geometry of unit 260 in T2 and T3 suggests it is a colluvial wedge resulting from event E3 that post-dates the placement of bedrock over unit 270 ([Figures 9B, 10](#)). An alternative interpretation is that units 270 and 260 represent the same colluvial wedge deposit split

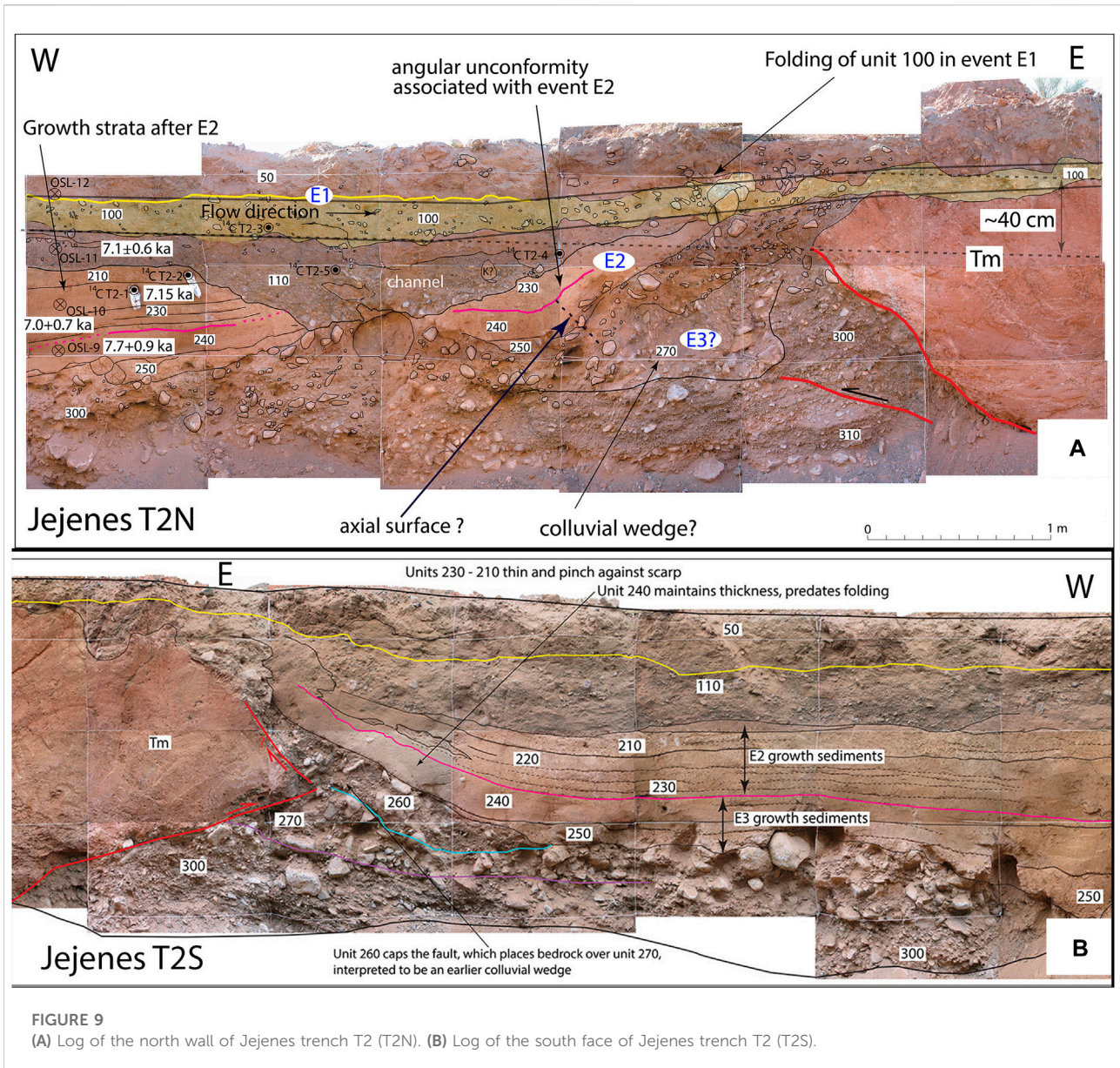
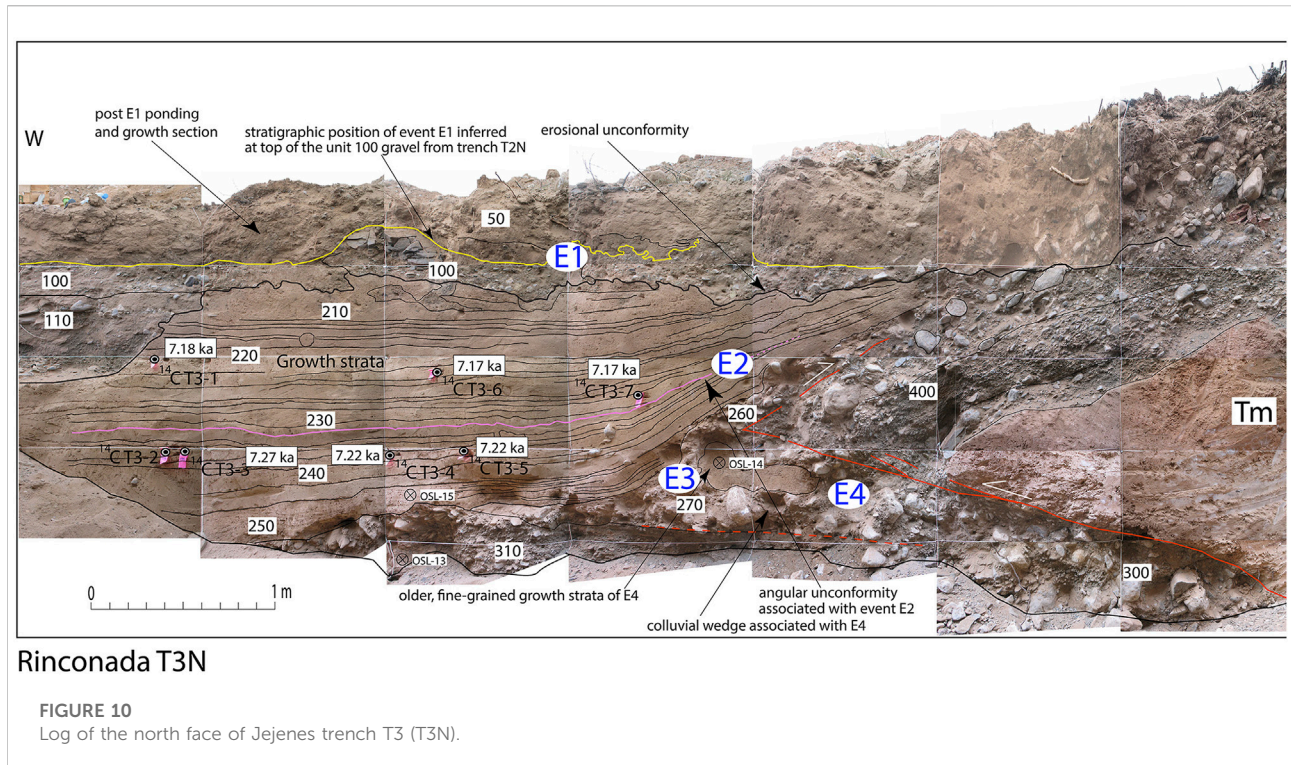


FIGURE 9
 (A) Log of the north wall of Jejenes trench T2 (T2N). (B) Log of the south face of Jejenes trench T2 (T2S).

by thrust-wedging of a blind thrust tip. In either interpretation, the event horizon is either between unit 270 and 260 or at the top of unit 260, neither of which has direct age control. Scarp formation in this event caused subsequent onlap of the fine-grained strata of units 255 up through 240 against the scarp.

In trench T1 (Figure 8), evidence for the three events following the abandonment of Q3 deposits is revealed by colluvial wedges and angular unconformities between units. Event E3 is interpreted to post-date the Q3 deposits of unit 300, with unit 260 forming a steep wedge on the scarp face (Figure 8). Scarp formation in this event caused subsequent deposition of the fine-grained strata of units 255 up through 240 against the scarp, which are interpreted as growth strata.

The two youngest events (E2 and E1) appear to have been essentially “blind”. Differential tilt and unconformities between successively younger units record progressive rotation of the fold limb exposed in all trench walls. Faults, in contrast, do not cut any units younger than 270. The E3 colluvial wedge, unit 260, is overlain by two units that have constant thickness across the fold axial trace. Unit 240 maintains thickness across an axial surface (fold hinge), whereas there is an angular unconformity between units 230 and 240, and the fine-grained units above 240 (210–230) thin or pinch-out onto the scarp. Unit 240 dips more steeply than unit 230. Deformation and folding of this fine-grained ponded alluvium deposited after E3 and before deposition of unit 230 thus provides evidence of folding and



scarp formation. Hence, we interpret E2 as a blind folding event between units 230 and 240.

The youngest event, E1, also appears to have been blind as the channel alluvium of unit 100 in T2N, possibly T3N, and unit 80 in T1 are deformed and folded, but the fault did not propagate to the surface except as a possible backthrust. Trench T2 was emplaced to capture this youngest event, where a small channel (unit 100) was defeated by recent motion; the channel expresses ~40 cm of vertical relief across the fault (Figure 9A), which is inferred to represent about 80 cm of dip-slip on a 30° dipping fault at depth below the base of the trench.

Ages of the Quebrada Jejenes events

We analyzed 25 individual samples of detrital charcoal and 12 OSL samples from the La Rinconada trenches to establish the ages of units 255 up through 80 (Table 2; Supplementary Table S3 in Supplementary Material). However, the age results for most of the ^{14}C ages are problematic from two perspectives. First, all of the charcoal samples from units 270 up through 220 yielded essentially the same age, which ranged from ~7.2 to 7.8 ka, with no apparent stratigraphic coherence. This could be interpreted as the very rapid deposition of these strata. However, the OSL sample from unit 270 yielded an age of 4.5 ± 0.4 ka, and another sample from unit 240 yielded an age of 3.7 ± 0.5 ka (Table 2). As OSL ages based on multiple grain aliquots, as is the case here, are typically considered maximum ages because of

the potential for partial bleaching of some of the grains, it appears that all of the charcoal was eroded from or derived from a common source immediately after event E3, which was most likely an anthropic source considering the arid climate of the region. The majority of the OSL ages also appear to have a partial bleach signal, as the calibrated ages based on a two-mixing model are older than one or more ages from underlying strata when considering their uncertainties. Consequently, we used only the OSL and ^{14}C ages consistent with the sample stratigraphic order. Hence, only eight of the 37 ages were used in OxCal to calculate the ages of events E1 and E2.

Another noteworthy observation is that the base of the fine-grained section included in unit 270 (see T3N log, Figure 10) is mid-Holocene based on the one OSL age analyzed from this unit (OSL-14 sample, Table 2), and no older than 7.3 ka based on the charcoal ages. In contrast, Hedrick et al. (2013) estimated the age of the Q3 alluvium at about 25–29 ka based on ^{10}Be TCN dating of four clast-samples from two sites on the Q3 surface. The mean ~25 ka TCN ages of Q3a, Q3b, and Q1c are indistinguishable from one another (Hedrick et al., 2013). The clast ages and overlapping mean ages suggest that the ~25 ka equivalent ^{10}Be concentration reflects inherited ages in the surface samples. Thus, the TCN samples indicate the surface age must be lesser and the OSL data provide a more realistic bound on the age for terrace formation. The unit 300 deposits did not have buried soil or other evidence of exposure of the sediments that could account for a significant period of surface exposure, whereas the Q3 surface soil described in Hedrick et al. (2013) included a 30-cm-thick gypsic

TABLE 2 ^{14}C and OSL ages from the Jejenes trench exposures and their relationship to interpreted events. Radiocarbon ages were calibrated using OxCal v4.4.4 (Bronk-Ramsey, 2021; atmospheric data from Reimer et al., 2020).

Event	Unit	^{14}C sample #	OSL sample #	Age (ka BP)
	50		T2-OSL12	4.0 ± 0.4
	80	T1-10 and T1-9		$6.0 \pm 0.3, 2.8 \pm 0.1$
			T1-OSL8	5.8 ± 0.4
Event E1				
	100	T1-5 and T1-8		$2.6 \pm 0.2, 2.8 \pm 0.1$
			T1-OSL7	6.6 ± 0.4
	110		T2-OSL11	4.5 ± 0.3
	120		T1-OSL6	3.4 ± 0.2
			T1-OSL5	3.5 ± 0.3
Non-tectonic depositional break				
	220	T2-1, T3-1, and T3-6		$7.15 \pm 0.1, 7.18 \pm 0.1, 7.17 \pm 0.1$
			T2-OSL10	5.9 ± 0.4
	230	T3-7, T1-2P, and T1-1		$7.17 \pm 0.1, 7.35 \pm 0.1, 7.31 \pm 0.1$
		T1-18, T1-21, and T1-22		$7.33 \pm 0.1, 7.37 \pm 0.1, 7.59 \pm 0.1$
		T1-4		7.82 ± 0.1
Event E2				
	240	T3-3, T3-4, and T3-5		$7.43 \pm 0.1, 7.22 \pm 0.1, 7.22 \pm 0.1$
		T1-13, T1-14, and T1-19		$7.15 \pm 0.1, 7.27 \pm 0.1, 7.83 \pm 0.1$
		T1-20 and T1-26		$7.27 \pm 0.1, 7.22 \pm 0.1$
			T1-OSL3, T1-OSL4	$3.7 \pm 0.5, 8.0 \pm 0.5$
	250	T1-15		7.41 ± 0.1
			T2-OSL9	6.2 ± 0.4
	255	T1-25, T1-24, and T1-23		$7.48 \pm 0.1, 7.31 \pm 0.1, 7.27 \pm 0.1$
	270		T1-OSL0	4.5 ± 0.4
Event E3				
	300/Q3 deposits		T3-OSL13	
	310			

horizon (typical for soils in this hyperarid region). The bound on the older possible age for Q3 is more readily defended using the 12–16 ka age of the youngest Q3 clasts, which we adopt herein.

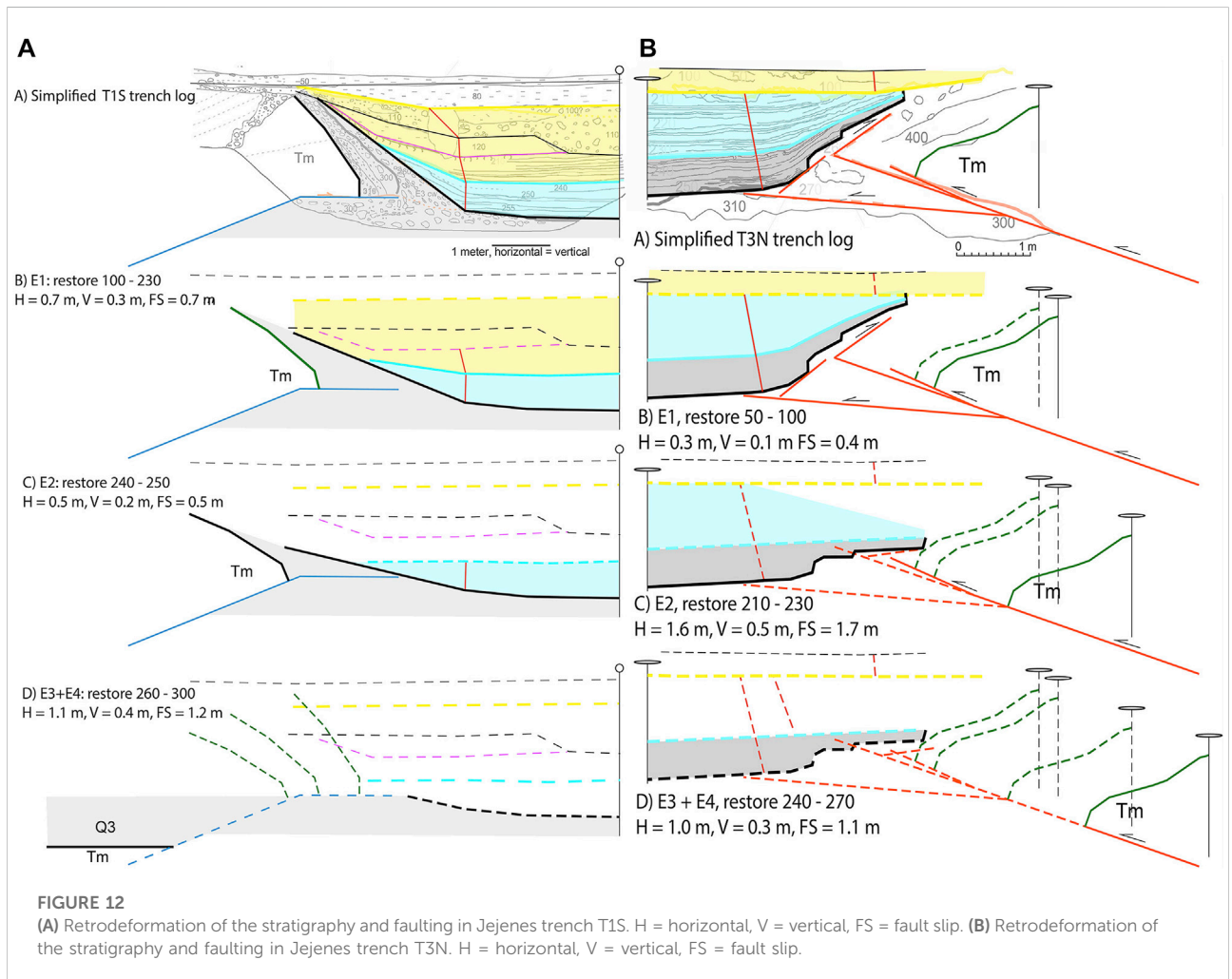
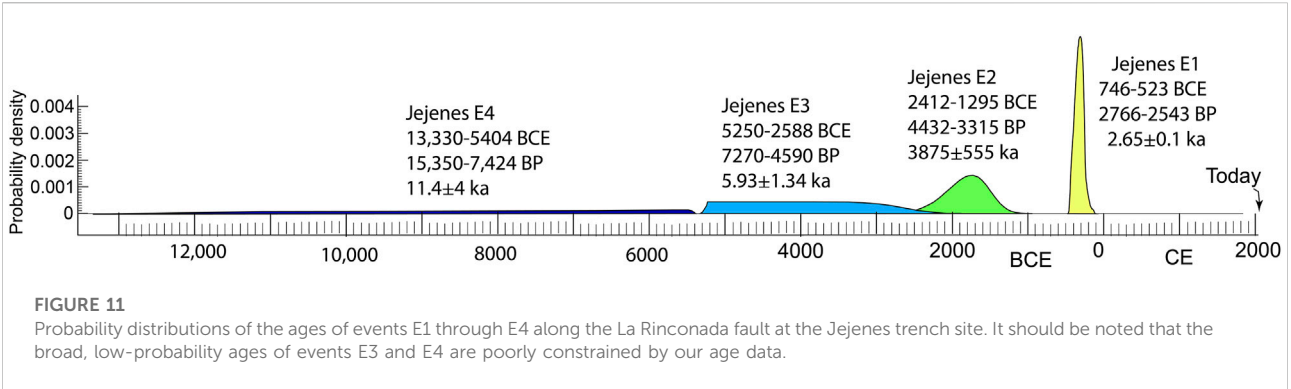
There are no direct age data that bracket the timing of events E3 and E4. However, the age of the Q3 deposits, the OSL date for unit 270, and the ^{14}C dates from unit 255 constrain the ages of events E3 and E4. A scarp produced in event E3 induced the fine-grained deposition of unit 270, which has an OSL date of 4.5 ± 0.5 ka (Table 2). Unit 255 yielded three detrital charcoal ages between ~ 7.3 and 7.5 ka. Assuming that all of the charcoal was already in the system and was simply eroded and deposited against the scarp, the timing of E3 is bracketed to between 4.5 ± 0.5 and ~ 7.3 ka. Event E4 must have occurred after abandonment of the Q3 surface, which has a maximum age of 12–16 ka. Hence, we place the timing of E4 between ~ 7.3 ka and 12–16 ka.

The ages of events E1 and E2 are well-determined by our age data. In contrast, event E3 is moderately constrained and E4 is poorly constrained. The results of the OxCal model are presented in Figure 11; the model itself is described in the Supplementary

Material. Event E1 occurred at about 2.7 ± 0.01 ka and E2 at 3.9 ± 0.6 ka, indicating a temporal cluster, which we discuss as follows. The pre-penultimate event (E3) occurred at about 5.9 ± 1.3 ka, whereas the timing of E4 is estimated at 11.4 ± 4 ka. It is to be noted that the age of event E1 is bound by only one ^{14}C age from the deposits that cap the event, and if that charcoal sample had inherited age or was reworked, then the actual age of E1 could be lesser. Notably, Instituto Nacional de Prevención Sísmica (1982) excavated a trench along the La Rinconada fault and determined that the most recent rupture post-dated a sandy deposit with a ^{14}C age of $2,505 \pm 160$ years BP (calibrated to 2.6 ± 0.4 ka) but no capping age; we use their date in our model.

Constraints on slip per event at Quebrada Jejenes

Balanced, sequential restoration of growth strata constrains the horizontal shortening and fault slip associated with the



E1–E3 paleoearthquakes (Figure 12). Restoration implicitly assumes a particle path, or vector, between the deformed and undeformed states, which has implications for changes in fold shape in sequential steps (Suppe et al., 1997). Geologically

untenable artifacts, such as localized shear along unconformities or the creation of new folds, result from incorrect choices of particle path. Particle paths parallel to fold hinges in folds formed due to kink-bed migration forms

the basis of the vector restoration method (Suppe et al., 1997; Novoa et al., 2000). We employed the vector restoration method because it simultaneously conserves bed length and area and honors unconformable contact relationships.

Figure 12A shows the sequential reconstruction of the growth strata exposed in trench T1 across the western fault strand (Figure 4). Returning unit 80 and younger to horizontal reveals shortening and fault slip accompanied event E1. A total of 50-cm horizontal shortening and fault slip are recovered when units 230 and younger are restored. The final stage of restoration matches unit 300 in the hanging wall and footwall (Figure 12A, panel D). In trench T3, event E4 is marked by unit 270 lying on unit 300; thus, this final restoration step includes both E3 and E4 events. It is not possible, based on the trench stratigraphic section in the hanging wall and footwall of T1, to constrain a discrete restoration step that separates the E3 from the E4 event. Slip in this step includes displacement associated with the fault reaching the surface. Horizontal shortening of 2.7 m and 2.9 m of the fault slip results from the restoration of units 260–240 to horizontal. If the total fault slip is divided equally between E3 and E4, which is an assumption, then the amount of slip at T1 in E3 and E4 is about the same at ~1.45 m.

Shortening and fault slip derived from the restoration of T3 across the eastern fault strand contrast with those of T1 (Figure 12B). Restoration of unit 100 yields 0.3 m of horizontal shortening and 0.4 m of fault slip during event E1. Horizontal shortening and fault slip in E2 are 1.6 m and 1.7 m, respectively, due restoration of units 230 and younger. Shortening and slip associated with E3 + E4 are a minimum, as unit 400 is the oldest in the hanging wall and has no correlative in the footwall for restoration. Less horizontal shortening (1.0 m) and fault slip (1.7 m) are revealed by the restoration of units 260–240 and the structural overlap of bedrock on unit 300 (Figure 12B panel D).

We infer that the western and eastern fault strands rupture together in earthquakes because they are interpreted to merge at ~150 m below the Earth's surface (Figure 4B). Whereas this conservative interpretation is consistent with the resolution of the age data, more complicated scenarios cannot be ruled out. Combining the displacement from the eastern and western strands suggests that 1.0 m of horizontal shortening and 1.1 m of fault slip accompanied event E1. The western strand absorbed more shortening than the eastern strand in this event. In contrast, the eastern strand accounts for 75% of the 2.1 m of horizontal shortening and 2.2 m of fault slip in E2. Roughly similar amounts of shortening and fault slip (~1 m) characterize events E1, E3, and E4. Event E2, in contrast, is relatively larger by a factor of ~2x, given the ~2 m slip recovered in the restoration of the two trenches.

The retrodeformations suggest that the La Rinconada fault accounts for 6.7 m of shortening and 7.3 m of fault slip, given the formation of Q3 in less than ~12–16 ka. This yields a minimum shortening and slip rate of 0.4–0.6 mm/yr as the result of four

earthquakes. A 0.4–0.6 mm/yr, the shortening rate compares favorably with the 0.4 mm/yr shortening rate determined at sites to the north and south of Quebrada Jejenos along strike on the La Rinconada fault (Rimando et al., 2019).

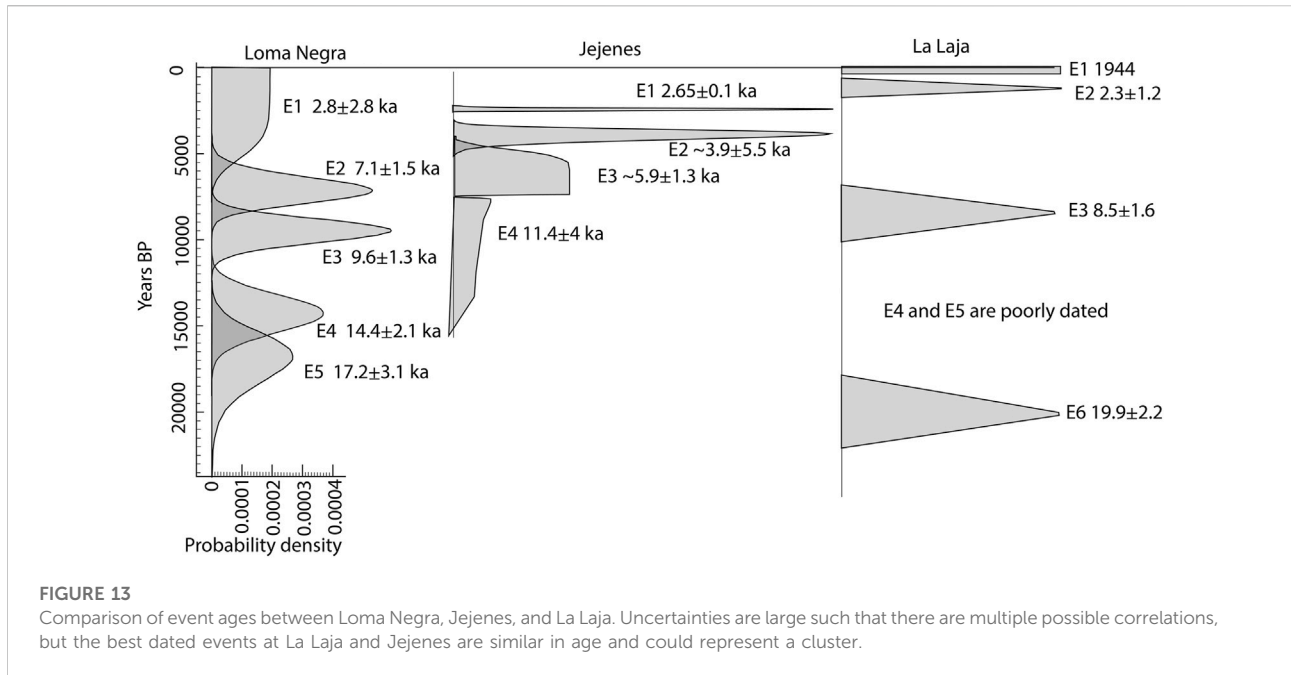
Discussion

We present evidence for five surface ruptures along the Marquesado fault over the past 17.2 ± 3.1 ka at the Loma Negra site, with the most recent event occurring in the past 2.8 ± 2.8 ka. The average recurrence interval at the Loma Negra site is 3.6 ka, with intervals ranging from 2.5 to 4.8 ka. Four events on the La Rinconada fault are recognized at the Quebrada Jejenos site that post-date deposition and abandonment of the 12–16 ka Q3 terrace (Hedrick et al., 2013). Thus, both sites document a recurrence interval of several thousand years, similar to that documented for the La Laja fault on the eastern flank of Sierra de Villicum north of San Juan (Rockwell et al., 2014).

We determined minimum and maximum post unit 300 displacement at Loma Negra to be 4.5–5 m and 10–12 m, respectively. The 10–12 m is likely an over-estimate because it assumes that the fan surfaces correlate across the fault, which they do not based on the soil development into the respective fan deposits. The lower bound is based on the minimum displacement exposed in the trench walls (Figures 5, 6). Assuming the lower bound is close to correct, which is the most conservative estimate, the average displacement per event is on the order of 1 m for the single strand that we studied. However, the events were not all the same size, and the youngest event appears to be smaller than most, assuming that the other Loma Negra strands did not also slip in the most recent event.

At the Quebrada Jejenos site, we reconstructed displacement per event individually for each fault strand and then summed it across the zone. We determined that about 7.3 m of post-Q3 fault slip has occurred, which equates to 6.7 m of shortening. The most recent event was the smallest, with only about 1 m of fault slip. Hence, the post-Q3 fault displacements are comparable at both Loma Negra and Quebrada Jejenos, which implies the minimum amount of fault slip at depth. Also notable is that the most recent event was smaller than average at both sites. The M_w 7.0 1944 San Juan earthquake (Alvarado and Beck, 2006) also produced smaller than average displacement at La Laja (Rockwell et al., 2014); together, this indicates that the Eastern Precordilleran thrust system is likely capable of producing earthquakes larger than what occurred in 1944.

Figure 13 compares the rupture history of the Marquesado-La Rinconada fault zone flanking the Sierra Chica de Zonda with the La Laja fault flanking the Sierra Villicum, which ruptured in 1944. It is plausible that the most recent event at Loma Negra and Jejenos represents an earthquake that ruptured the entire



Marquesado–La Rinconada fault in concert. However, as the most recent event at both sites had smaller than average displacement, we consider it more likely that these may have been separate events that were closely spaced in time. The large displacement determined for older events, in contrast, suggests that the entire system may have ruptured in some earlier earthquakes.

Comparison of these new events with the La Laja fault paleoseismic record does not suggest coeval ruptures with either the Marquesado or La Rinconada fault systems. However, the most recent events along the Marquesado–La Rinconada fault system apparently preceded the ca. 2.2 ka penultimate event along the La Laja fault by only a few centuries or less. If correct, the observations suggest that at least some earthquakes cluster in time along the Eastern Precordilleran fault system and may result from stress loading when an adjacent fault segment fails, as occurred with the North Anatolian fault in Turkey (Stein et al., 1997). The 1944 earthquake may be a harbinger of future activity along the range front south of San Juan. Additional paleoseismic work with better age control may help shed light on these possible correlations.

Eight years after the 1944 San Juan earthquake, there was an M_w 6.8 earthquake that occurred ~30 km to the SW, beneath the valley to the east of the northern end of Sierra Chica de Zonda (Tello and Perucca, 1993; Alvarado and Beck, 2006). It is tempting to argue that the 1952 event was triggered by the 1944 earthquake, as occurred in the 1977 foreshock-main shock Cauçete earthquake sequence (Langer and Hartzell, 1996). Whereas rupture of the La Laja fault unequivocally occurred in 1944 (Castellanos, 1944; Groeber, 1944; Harrington, 1944), assigning the 1952 event to a known

structure is problematic. The 1952 event had a strike-slip mechanism, involving nodal planes with a 40° strike and 75° dip, and a 301°-striking plane, 61° dip, and 12 km depth (Alvarado and Beck, 2006). The 301°-striking plane parallels the strike of the Paleozoic bedrock exposed near the Loma Negra site (Figure 3). Geomorphic and trench observations at the Loma Negra site, however, indicate that active faulting at the surface takes place on north-striking bedding-parallel dip-slip faults in the Neogene bedrock that do not align with either plane of the focal mechanism. The 12 km depth presents an additional complication in that structural, stratigraphic, and seismic data suggest that the Eastern Precordilleran basal décollement lies at ~5 km depth (Baldis et al., 1982; Allmendinger et al., 1990; von Gosen, 1992; Gardini, 1993; Zapata and Allmendinger, 1996; Ramos et al., 1997; Giampaoli and Cegarra, 2003; Vergés et al., 2007; Richard et al., 2019). These constraints suggest that the 1952 event occurred below the décollement. Whereas stress transfer following the 1944 event may have triggered the 1952 earthquake (i.e., Stein, 1999), whether a lateral ramp or other deep transverse structure links the deeper structure beneath Sierra Chica de Zonda with the deep structure beneath Sierra de Villicum is uncertain.

Paleoearthquakes on the Marquesado and La Rinconada fault systems are unequivocally demonstrated by folding of Quaternary terraces, fans, and fault offset in trench exposures, and geophysical data (Figures 2–4) (Instituto Nacional de Prevención Sísmica, 1982; Bastías et al., 1984; Martos, 1987; Paredes and Bastías, 1987; Cardinali and Pereyra, 1998; Costa, 2009; Correa-Otto et al., 2018; Richard et al., 2019; Rimando et al., 2019). Two issues pose a challenge for using the paleoearthquake chronology to

constrain seismic hazards of the causative faults at depth. First, the active faults may be flexural-slip faults related to folding, backthrusts that utilized bedding in the upper crust, or reactivated older structures (Richard et al., 2019). Flexural-slip faulting typically manifests at the surface as a series of close, regularly spaced faults (Rockwell et al., 1984; Rockwell, 1988; Li et al., 2017). Constraint on coseismic slip on the source fault from secondary faulting is non-trivial, as it requires models that link flexural-slip faulting in a fold limb to fault-related fold growth in earthquakes on the primary seismic source fault (Le Béon et al., 2014). At the La Laja site, numerous regularly spaced faults deform terraces across a broad region within the limb of a multi-kilometer scale fold. Localization of slip on a single fault and warping of terraces across a hanging wall monocline at La Rinconada, in contrast, imply a different linkage between surface faulting and the primary seismic source at depth. Displacement on a backthrust formed in the limb of a structural wedge of a fault-related fold is directly proportionate to the primary fault at depth (Kraig et al., 1987; Medwedeff, 1992). The large magnitude and localization of slip on a single structure favor an interpretation that the La Rinconada fault is a backthrust with a hanging wall flat on footwall flat geometry at Quebrada Jejenes (Figure 4) (Richard et al., 2019). Thus, the slip per event at the site is likely a proxy for slip on the source fault in each event.

A polydeformational history of faulting that extends back to the Paleozoic poses the second substantial challenge in constraining seismic hazard based on the topology of faults at the crustal-scale (Ramos et al., 2002). Two alternative models for the active faulting beneath Sierra de Villicum, which generated the 1944 San Juan earthquake and surface rupture on the La Laja fault, frame the open question of the depth and geometry of seismically active faulting beneath the Eastern Precordillera. In one model, the La Laja fault, range front faults of Sierras Chica de Zonda and Villicum, and other surface faults reflect earthquakes generated on a décollement in the upper crust (<20 km depth) (Siame et al., 2002; Alvarado and Beck, 2006; Ammirati et al., 2016). Alternatively, slip transfer from mid-crustal and deeper faults to the upper crustal décollement (Smalley et al., 1993; Vergés et al., 2007; Meigs and Nabelek, 2010) produces slip on shallow faults that reach the Earth's surface (Meigs et al., 2006; Rockwell et al., 2014). A model that includes both an upper crustal décollement and mid-crustal and deeper sources is required given historical seismicity (Kadinsky-Cade, 1985; Alvarado and Ramos, 2010; Meigs and Nabelek, 2010), yet limited knowledge of fault geometry hampers the use of surface deformation to place a constraint on source fault dimensions (except in a limited number of cases, e.g., Langer and Hartzell, 1996). Empirical relationships indicate that a $\sim M_w$ 6.5–7.5 event is consistent with the ~ 25 km length of the La Rinconada fault, the ~ 50 km-long extents of active folding and folding on the eastern flank of Sierra Chica de Zonda, and the meter-scale slip per event at the two sites (Wells and Coppersmith, 1994). Events as large as $\sim M_w$ 7.5 would also be consistent with the cumulative seismic

moment released by the 1977 Cauçete sequence (Langer and Hartzell, 1996).

Conclusion

The ages of the past five interpreted events at the Loma Negra site are E1 at 2.8 ± 2.8 ka, E2 at 7.1 ± 1.5 ka, E3 at 9.6 ± 1.3 ka, E4 at 14.4 ± 2.1 ka, and E5 at 17.2 ± 3.1 ka, which produced at least an average of 1 m of slip per event. At the Quebrada Jejenes sites, we documented the occurrence of four surface ruptures with event ages of 2.7 ± 0.1 ka, 3.9 ± 0.6 ka, 5.9 ± 1.3 ka, and 11.4 ± 4 ka. The observed displacements at the Loma Negra and Jejenes sites indicate that slip during event E1 was smaller than average at each site, which in turn suggests that these fault segments may have failed separately. Some earlier events, such as E3 and E4 at Jejenes and E2 at Loma Negra, resulted in larger displacement and may represent rupture along the entire Marquesado–La Rinconada fault system. The linkage of these faults along the Sierra Chica de Zonda has yet to be worked out.

Another main point is that the larger, earlier events appear to have been emergent, whereas some of the more recent, smaller events appear to have been blind. This suggests a relationship between the size of the causative earthquake and whether the displacement reaches the surface. The blind thrusting into fine-grained deposits that partly overlap the thrust scarp might also explain the poor expression of classic colluvial wedges.

Additional work is needed to better define the timing of the most recent event at both sites. The base of units 100 and 50 at Loma Negra and Jejenes Quebrada, respectively, may have been deformed by wedge thrusting, thus making the most recent event younger than suggested.

Data availability statement

The original contributions presented in the study are included in the article/Supplementary Material; further inquiries can be directed to the corresponding author.

Author contributions

TR and AM conceived the project, acquired the funding, participated in all aspects of the fieldwork, and co-wrote the manuscript. CC participated in the fieldwork and co-wrote the manuscript. LO participated in the fieldwork through the collection of OSL samples, oversaw the analysis of the OSL samples in the Cincinnati University Geochronology Laboratory, and participated in editing the manuscript. DR and EM participated in all aspects of the fieldwork and provided an internal review of the manuscript. MM processed and ran all OSL samples for the project, and AR conducted

additional fieldwork and field review and participated in the review of the manuscript.

Funding

This work was supported by NSF-EAR grants 0409443 and 0838538 to AM, NSF-EAR 0408494 and 0838375 to TR, NSF-EAR-0838344 to LAO, and Project CyT030318 from Universidad Nacional de San Luis to CC.

Acknowledgments

We thank the many landowners that allowed field access for this research. We thank Franz Livio, Franck Audemard, Stella Moreiras, and a reviewer for their excellent reviews and constructive comments.

Conflict of interest

DR was employed by the company Ecopetrol.

References

- Ahumada, E., and Costa, C. (2009). Antithetic linkage between oblique Quaternary thrusts at the Andean front, Argentine Precordillera. *J. South Am. Earth Sci.* 28, 207–216. doi:10.1016/j.jsames.2009.03.008
- Allmendinger, R. W., Figueroa, D., Snyder, D., Beer, J., Mpodozis, C., and Isacks, B. (1990). Foreland shortening and crustal balancing in the Andes at 30°S Latitude. *Tectonics* 9 (4), 789–809. doi:10.1029/tc009i004p00789
- Alvarado, P., and Beck, S. (2006). Source characterization of the san juan (Argentina) crustal earthquakes of 15 January 1944 (Mw 7.0) and 11 June 1952 (Mw 6.8). *Earth Planet. Sci. Lett.* 243, 615–631. doi:10.1016/j.epsl.2006.01.015
- Alvarado, P., Beck, S., Zandt, G., Araujo, M., and Triep, E. (2005). Crustal deformation in the south-central Andes backarc terranes as viewed from regional broad-band seismic waveform modelling. *Geophys. J. Int.* 163, 580–598. doi:10.1111/j.1365-246x.2005.02759.x
- Alvarado, P., Pardo, M., Gilbert, H., Miranda, S., Anderson, M., Saez, M., et al. (2009). “Flatslab subduction and crustal models for the seismically active Sierras Pampeanas region of Argentina,” in *Backbone of the Americas: Shallow subduction, plateau uplift, and ridge and terrane collision*. Editors S. M. V. A. KayRamos and W. R. Dickinson (Boulder, CO: Geological Society of America Memoir), 204, 261–278. doi:10.1130/2009.1204(12)
- Alvarado, P., and Ramos, V. (2010). La estructura Andica de las Sierras Pampeanas basada en los mecanismos focales de terremotos en su región Noroeste. *Revista Asociación Geológica Argentina* 67, 461–472.
- Ammirati, J.-B., Luján, S. P., Alvarado, P., Beck, S., Rocher, S., and Zandt, G. (2016). High-resolution images above the Pampean flat slab of Argentina (31–32°S) from local receiver functions: Implications on regional tectonics. *Earth Planet. Sci. Lett.* 450, 29–39. doi:10.1016/j.epsl.2016.06.018
- Audemard, F. (1999). Morpho-structural expression of active thrust fault systems in the humid tropical foothills of Colombia and Venezuela. *Z. für Geomorphol.* 118, 1–18.
- Baby, P., Rochat, P., Mascle, G., and Hérail, G. (1997). Neogene shortening contribution to crustal thickening in the back arc of the central Andes. *Geol.* 25 (10), 883–886. doi:10.1130/0091-7613(1997)025<0883:nsctct>2.3.co;2
- Baldis, B., Beresi, M., Bordonaro, O., and Vaca, A. (1982). Síntesis evolutiva de la Precordillera Argentina. *Congr. Latinoam. Geol.* 5 (4), 399–445.
- Bastías, H., Weidmann, N., and Pérez, M. (1984). “Dos zonas de fallamiento Pliocuaternario en la Precordillera de San Juan,” in 9° Congreso Geológico Argentino, Actas, Bariloche, September, 1984, 329–341.
- Bellahsen, N., Sebrier, M., and Siame, L. (2016). Crustal shortening at the sierra pie de Palo (Sierras Pampeanas, Argentina): Near-surface basement folding and thrusting. *Geol. Mag.* 153 (5/6), 992–1012. doi:10.1017/S0016756816000467
- Bès de Berc, S., Soula, J. C., Baby, P., Souris, M., Christophoul, F., and Rosero, J. (2005). Geomorphic evidence of active deformation and uplift in a modern continental wedge-top-foredeep transition: Example of the eastern Ecuadorian Andes. *Tectonophysics* 399, 351–380. doi:10.1016/j.tecto.2004.12.030
- Blanc, P., and Perucca, L. (2017). Tectonic and climatic controls on the late Pleistocene to Holocene evolution of Paleolake Ullum-Zonda in the Precordillera of the central Andes, Argentina. *Quat. Res.* 88, 248–264. doi:10.1017/qua.2017.50
- Bronk-Ramsey (2021). OxCal v4.4, r.5. Available at: <https://c14.arch.ox.ac.uk/oxcal/OxCal.html>.
- Brooks, B. A., Bevis, M., Whipple, K., Arrowsmith, R., FosterZapata, J. T., Kendrick, E., et al. (2011). Orogenic-wedge deformation and potential for great earthquakes in the central Andean backarc. *Nat. Geosci.* 4, 380–383. doi:10.1038/ngeo1143
- Brooks, B., Bevis, M., Smalley, R., Kendrick, E., Manceda, R., Lauría, E., et al. (2003). Crustal motion in the southern Andes (26°–36°S): Do the Andes behave like a microplate? *Geochem. Geophys. Geosyst.* 4, 1–14. doi:10.1029/2003gc000505
- Cahill, T., and Isacks, B. (1992). Seismicity and shape of the subducted Nazca plate. *J. Geophys. Res.* 97 (B12), 17503–17529. doi:10.1029/92jb00493
- Cardinali, A., and Pereyra, B. (1998). “Plegamiento por flexión de falla en el Cuaternario de la sierra de Marquesado, Precordillera Oriental, San Juan,” in 10th Congreso Latinoamericano de Geología, Buenos Aires, October, 1998, 23–28.
- Castellanos, A. (1944). in *Anotaciones preliminares con motivo de una visita a la ciudad de San Juan a propósito del terremoto del 15 de enero de 1944*, U.N.L (Rosario, Argentina: Inst. Fis. Y Geol. Pub), 21.
- Correa-Otto, S., Ariza, J., Lince Klinger, F., Giménez, M., and Lopez Hidalgo, A. (2018). Analysis of neotectonic structures in the Eastern Precordillera of Argentina in relation to seismic hazard by the application of integrated geophysical methods. *Tectonophysics* 728–729, 23–33. doi:10.1016/j.tecto.2018.02.005
- Costa, C., Ahumada, E., Gardini, C., Vazquez, F., and Diederix, H. (2014). Quaternary shortening at the orogenic front of the central Andes of Argentina: The Las Peñas thrust system. *Geol. Soc. Sp. Publ.* 399, 245–266. doi:10.1144/SP399.5
- Costa, C., Audemard, F., Bezerra, F., Lavenue, A., Machette, M., and Paris, G. (2006). An overview of the main Quaternary deformation of South America. *Rev. Asoc. Geol. Argent.* 61, 461–479.

The remaining authors declare that the research was conducted in the absence of any commercial or financial relationships that could be construed as a potential conflict of interest.

Publisher's note

All claims expressed in this article are solely those of the authors and do not necessarily represent those of their affiliated organizations, or those of the publisher, the editors, and the reviewers. Any product that may be evaluated in this article, or claim that may be made by its manufacturer, is not guaranteed or endorsed by the publisher.

Supplementary material

The Supplementary Material for this article can be found online at: <https://www.frontiersin.org/articles/10.3389/feart.2022.1032357/full#supplementary-material>

- Costa, C. (2009). "Falla La Rinconada (AR-22)," in *Proyecto Multinacional Andino (PMA)*, 2009. *Atlas de deformaciones cuaternarias de los Andes*, SERNAGEOMIN (Santiago, Amsterdam: Publicación Geológica Multinacional), 104–110.
- Costa, C., Gardini, C., Diederix, H., and Cortés, J. (2000). The andean orogenic front at sierra de Las peñas-las Higuera, Mendoza, Argentina. *J. South Am. Earth Sci.* 13, 287–292. doi:10.1016/S0895-9811(00)00010-9
- Costa, C., Owen, L., Johnson, W., and Kirby, E. (2021). Quaternary activity and seismogenic potential of the sierra Chica fault system, pampean ranges of Argentina. *J. South Am. Earth Sci.* 110, 103328. doi:10.1016/j.jsames.2021.103328
- Costa, C., Owen, L., Ricci, W., Johnson, W., and Halperin, A. (2018). Holocene activity and seismogenic capability of intraplate thrusts: Insights from the Pampean Ranges, Argentina. *Tectonophysics* 737, 57–70. doi:10.1016/j.tecto.2018.05.002
- Costa, C., Rockwell, T., Paredes, J., and Gardini, C. (1999). *Quaternary deformations and seismic hazard at the andean orogenic front (31°–33°, Argentina): A paleoseismological perspective. IV international symposium on andean geodynamics, extended abstracts: 187–191*. Paris: IRD.
- Costa, C., Schoenbohm, L., Brooks, B., Gardini, C., and Richard, A. (2019). Assessing quaternary shortening rates at an andean frontal thrust (32°30'S), Argentina. *Tectonics* 38, 3034–3051. doi:10.1029/2019TC005564
- Cristallini, E. O., and Ramos, V. A. (2000). Thick-skinned and thin-skinned thrusting in the La ramada fold and thrust belt: Crustal evolution of the high Andes of san juan, Argentina (32°SL). *Tectonophysics* 317 (3/4), 205–235. doi:10.1016/S0040-1951(99)00276-0
- Dumont, J. F. (1996). Neotectonics of the Subandes-Braz, ilian craton boundary using geomorphological data: The Maraón and Beni basins. *Tectonophysics* 257, 137–151. doi:10.1016/0040-1951(95)00200-6
- Engdahl, R., van der Hilst, R., and Buland, R. (1998). Global teleseismic earthquake relocation with improved travel times and procedures for depth relocation. *Bull. Seismol. Soc. Am.* 88, 722–743.
- Fielding, E. J., and Jordan, T. E. (1988). Active deformation at the boundary between the Precordillera and Sierras Pampeanas, Argentina, and comparison with ancient rocky mountain deformation. *Mem. - Geol. Soc. Am.* 171, 143–163.
- Galindo, C., Casquet, C., Rapela, C., Pankhurst, R. J., Baldo, E., and Saavedra, J. (2004). Sr, C and O isotope geochemistry and stratigraphy of Precambrian and lower Paleozoic carbonate sequences from the Western Sierras Pampeanas of Argentina: Tectonic implications. *Precambrian Res.* 131, 55–71. doi:10.1016/j.precamres.2003.12.007
- Gardini, M. (1993). "Estructura superficial y profunda del valle de Zonda, Precordillera de San Juan," in 12th Congreso Geológico Argentino, Actas, Mendoza, September, 1993, 93–99.
- Giampaoli, P., and Cegarra, M. (2003). Análisis estructural del extremo sur de la Precordillera Central Sanjuanina. *Rev. Asoc. Geol. Argent.* 58, 49–60.
- Groeber, P. (1944). Movimientos tectónicos contemporáneos y un nuevo tipo de dislocaciones. *Notas Mus. La Plata* 9, 363–375.
- Gutscher, M.-A., Spakman, W., Bijwaard, H., and Engdahl, E. R. (2000). Geodynamics of flat subduction; seismicity and tomographic constraints from the Andean margin. *Tectonics* 19 (5), 814–833. doi:10.1029/1999tc001152
- Harrington, H. (1944). *Volcanes y terremotos*. Buenos Aires: Pleamar, 251.
- Hedrick, K., Owen, L., Rockwell, K., Meigs, A., Costa, C., Ahumada, E., et al. (2013). Timing and nature of alluvial fan and strath terrace formation in the Eastern Precordillera of Argentina. *Quat. Sci. Rev.* 80, 143–168. doi:10.1016/j.quascirev.2013.05.004
- Instituto Nacional de Prevención Sísmica (1982). *Microzonificación sísmica del Valle de Tulum, Provincia de San Juan*. San: Resumen ejecutivo, 120.
- Jordan, T., and Allmendinger, R. (1986). The Sierras Pampeanas of Argentina; a modern analogue of Rocky Mountain foreland deformation. *Am. J. Sci.* 286, 737–764. doi:10.2475/ajs.286.10.737
- Jordan, T., Isacks, B., Allmendinger, R., Brewer, J., Ramos, V., and Ando, C. (1983). Andean tectonics related to geometry of subducted Nazca plate. *Geol. Soc. Am. Bull.* 94, 341. doi:10.1130/0016-7606(1983)94<341:artgo>2.0.co;2
- Kadinsky-Cade, K. (1985). *Seismotectonics of the Chile margin and the 1977 Cauce earthquake of western Argentina*. Cornell University, 253.
- Karlsson, K. W., Rockwell, T. K., Fletcher, J. M., Figueiredo, P. M., Rosas, J. F. C., Gontz, A. M., et al. (2021). Large Holocene ruptures on the Cañada David detachment, Baja California, Mexico; implications for the seismogenesis of low-angle normal faults. *Earth Planet. Sci. Lett.* 570, 117070. doi:10.1016/j.epsl.2021.117070
- Kendrick, E., Bevis, M., Smalley, R., and Brooks, B. (2001). An integrated crustal velocity field for the Central Andes. *Geochim. Geophys. Geosyst.* 2, 2001GC000191.
- Kendrick, E., Bevis, M., Smalley, R. F., Jr., Cifuentes, O., and Galbán, F. (1999). Current rates of convergence across the Central Andes; estimates from continuous GPS observations. *Geophys. Res. Lett.* 26 (5), 541–544. doi:10.1029/1999gl900040
- Kraig, D. H., Wiltschko, D. V., and Spang, J. H. (1987). Interaction of basement uplift and thin-skinned thrusting, Moxa arch and the western overthrust belt, Wyoming: A hypothesis. *Geol. Soc. Am. Bull.* 99, 654–662. doi:10.1130/0016-7606
- Langer, C. J., and Hartzell, S. (1996). Rupture distribution of the 1977 western Argentina earthquake. *Phys. Earth Planet. Interiors* 94, 121–132. doi:10.1016/0031-9201(95)03080-8
- Le Béon, M., Suppe, J., Jaiswal, M. K., Chen, Y. G., and Ustaszewski, M. E. (2014). Deciphering cumulative fault slip vectors from fold scarps: Relationships between long-term and coseismic deformations in central Western Taiwan. *J. Geophys. Res. Solid Earth* 119 (7), 5943–5978. doi:10.1002/2013jb010794
- Li, T., Chen, J., Thompson Jobe, J. A., and Burbank, D. W. (2017). Active flexural-slip faulting: Controls exerted by stratigraphy, geometry, and fold kinematics. *J. Geophys. Res. Solid Earth* 122 (10), 8538–8565. doi:10.1002/2017jb013966
- Lombardo, U., and Grützner, C. (2021). Tectonic geomorphology and active faults in the Bolivian Amazon. *Glob. Planet. Change* 203, 103544. doi:10.1016/J.GLOPLACHA.2021.103544
- Martos, L. M. (1987). Evidencia de movimientos neotectónicos en una terraza de edad Holocena, La Rinconada-San Juan. 10° Congreso Geológico Argentino. *San Miguel Tucumán. Actas* 1, 263–265.
- Medwedeff, D. (1992). "Geometry and kinematics of an active, laterally propagating wedge thrust, wheeler ridge, California," in *Geology of fold and thrust belts, chapter: Geometry and kinematics of an active, laterally propagating wedge thrust, wheeler ridge, California*. Editors S. Mitra and G. W. Fisher (Baltimore: The Johns Hopkins University Press), 3–28.
- Meigs, A. J., and Nabelek, J. (2010). Crustal-scale pure shear foreland deformation of western Argentina. *Geophys. Res. Lett.* 37 L11304, 5. doi:10.1029/2010GL043220
- Meigs, A., Krugh, W. C., Schiffman, C., Vergés, J., and Ramos, V. (2006). Refoldin of thin-skinned thrust sheets by active basement-involved thrust faults in the Eastern Precordillera or western Argentina. *Rev. Asoc. Geol. Argent.* 61 (4), 589–603.
- Novoa, E., Suppe, J., and Shaw, J. H. (2000). Inclined-shear restoration of growth folds. *Am. Assoc. Petroleum Geol. Bull.* 84 (6), 787–804.
- Oncken, O., Hindle, D., Kley, J., Elger, K., Victor, P., and Schemmann, K. (2006). "Deformation of the Central Andean upper plate system - Facts, fiction, and constraints for plateau models," in *The Andes - Active Subduction Orogeny, (Frontiers in Earth Sciences)*. Editors O. Oncken, G. Chong, G. Franz, P. Giese, H.-J. Götze, V. Ramos, et al. (Springer), 3–27. doi:10.1007/978-3-540-48684-8_1
- Ortiz, A., and Zambrano, J. J. (1981). "La provincia geológica Precordillera orientada," in 18º Congreso Geológico Argentino, Actas San Luis, San Luis, September, 1981, 59–74.
- Paredes, J., and Bastias, H. (1987). "Formas y rangos de alzamiento del sector norte de la sierra Chica de Zonda-San Juan - R. Argentina," in 10th Congreso Geológico Argentino, Tucuman, September, 1987, 279–282.
- Paredes, J., and Perucca, L. (2000). Fallamiento cuaternario en la depresión de Matagusanos, San Juan, Argentina. *Rev. Asoc. Geol. Argent.* 55 (1-2), 23–30.
- Perucca, L., and Vargas, N. (2014). Neotectónica de la provincia de San Juan, centro-oeste de Argentina. *Bol. Soc. Geol. Mex.* 66, 291–304. doi:10.18268/bsgm2014v66n2a6
- Ramos, V. (1988). "The tectonics of the Central Andes: 30° to 33°S latitude," in *Processes in continental lithospheric deformation*, Santiago, November, 1997. Editors S. Clark and C. Burchfiel (Boulder, CO: Geological Society of America, Special Paper), 218, 31–54.
- Ramos, V. A., Cegarra, M. I., Lo Forte, G., and Comínguez, A. (1997). "El frente orogénico de la sierra de Pedernal (san juan, Argentina): Su migración a través de los depósitos sinorogénicos," in Actas 8º Congreso Geológico Chileno, 1709–1713.
- Ramos, V. A., Cristallini, E. O., and Pérez, D. J. (2002). The pampean flat-slab of the central Andes. *J. S. Am. Earth Sci.* 15, 59–78. doi:10.1016/S0895-9811(02)00006-8
- Ramos, V. (2009). Anatomy and global context of the Andes: Main geologic features and the Andean orogenic cycle. *Mem. Geol. Soc. Am.* 204, 31–65.
- Ramos, V. A., and Vujovich, G. (2000). Hoja Geológica san juan, serv. *Geol. Min. Argent. Bol.* 245, 1–82.
- Reimer, P., Austin, W., Bard, E., Bayliss, A., Blackwell, P., Bronk Ramsey, C., et al. (2020). The IntCal20 Northern Hemisphere radiocarbon age calibration curve (0–55 cal kBP). *Radiocarbon* 62, 725–757. doi:10.1017/rdc.2020.41
- Richard, A., Costa, C., Giambiagi, L., Moreno, C., Ahumada, E., and Vázquez, F. (2019). Neotectónica del extremo austral de la falla La Rinconada, Precordillera Oriental, provincia de San Juan. *Rev. Asoc. Geol. Argent.* 76, 24–39.

- Rimando, J., Schoenbohm, L., Costa, C., Owen, L., Cesta, J., Richard, A., et al. (2019). Late quaternary activity of the La Rinconada fault zone, san juan, Argentina. *Tectonics* 38, 916–940. doi:10.1029/2018tc005321
- Rockwell, T. K., Keller, E. A., Clark, M. N., and Johnson, D. L. (1984). Chronology and rates of faulting of Ventura River terraces, California. *Geol. Soc. Am. Bull.* 95, 1466–1474. doi:10.1130/0016-7606(1984)95<1466:carofo>2.0.co;2
- Rockwell, T. K. (1988). Neotectonics of the san cayetano fault, transverse ranges, California. *Geol. Soc. Am. Bull.* 100 (4), 500–513. doi:10.1130/0016-7606(1988)100<0500:motscf>2.3.co;2
- Rockwell, T., Ragona, D., Meigs, A., Owen, L., Costa, C., and Ahumada, E. (2014). Inferring a thrust-related earthquake history from secondary faulting: A long rupture record of La Laja fault, san juan, Argentina. *Bull. Seismol. Soc. Am.* 104, 269–284. doi:10.1785/0120110080
- Soil Survey Staff (1993). “Soil survey manual,” in *USDA handbook No. 18*. Editors C. Ditzler, K. Scheffe, and H. C. Monger (Washington, D.C: Government Printing Office).
- Schmidt, S., Hetzel, R., Mingorance, F., and Ramos, V. (2011). Coseismic displacements and Holocene slip rates for two active thrust faults at the mountain front of the Andean Precordillera (~33°S). *Tectonics* 30, 30TC5011. doi:10.1029/2011TC002932
- Siame, L., Bellier, O., Sébrier, M., Bourlès, D., Leturmy, P., Pérez, M., et al. (2002). Seismic hazard reappraisal from combined structural geology, geomorphology and cosmic ray exposure dating analyses: The Eastern Precordillera thrust system (NW Argentina). *Geophys. J. Int.* 150, 241–260. doi:10.1046/j.1365-246x.2002.01701.x
- Smalley, R., Pujol, J., Regnier, M., Chiu, J.-M., Chatelain, J., Isacks, B., et al. (1993). Basement seismicity beneath the Andean Precordillera thin-skinned thrust belt and implications for crustal and lithospheric behavior. *Tectonics* 12, 63–76. doi:10.1029/92tc01108
- Stein, R. S., Barka, A., and Dieterich, J. D. (1997). Progressive failure on the North Anatolian fault since 1939 by earthquake stress triggering. *Geophys. J. Int.* 128, 594–604. doi:10.1111/j.1365-246x.1997.tb05321.x
- Stein, R. S. (1999). The role of stress transfer in earthquake occurrence. *Nature* 402, 605–609. doi:10.1038/45144
- Suppe, J., Sàbat, F., Muñoz, J. A., Poblet, J., Roca, E., and Vergés, J. (1997). Bed-by-bed fold growth by kink-band migration: Sant Llorenç de Morunys, eastern Pyrenees. *J. Struct. Geol.* 19 (3-4), 443–461. doi:10.1016/s0191-8141(96)00103-4
- Tello, G., and Perucca, L. (1993). “El sistema de fallamiento Precordillera Oriental y su relación con los sismos históricos de 1944 y 1952,” in 12° Congreso Geológico Argentino Actas, San Juan, Argentina, 1993, 246–251.
- Uliarte, E., Bastias, H., and Ruzycski, L. (1987). “Morfología y Neotectónica en el cerro La Chilca, Pedernal,” in Proceedings 10° Congreso Geológico Argentino. San Juan 1, 227–230.
- Vergés, J., Ramos, V. A., Meigs, A., Cristallini, E., Bettini, F. H., and Cortés, J. M. (2007). Crustal wedging triggering recent deformation in the Andean thrust front between 31°S and 33°S: Sierras Pampeanas-Precordillera interaction. *J. Geophys. Res.* 112 (B03S15), B03S15. doi:10.1029/2006jb004287
- von Gosen, W. (1992). Structural evolution of the Argentine Precordillera: The rio san juan section. *J. Struct. Geol.* 14 (6), 643–667. doi:10.1016/0191-8141(92)90124-f
- Weiss, J., Brooks, B., Arrowsmith, R., and Vergani, G. (2015). Spatial and temporal distribution of deformation at the front of the Andean orogenic wedge in southern Bolivia. *J. Geophys. Res. Solid Earth* 120, 1909–1931. doi:10.1002/2014JB011763
- Wells, D. L., and Coppersmith, K. J. (1994). New empirical relationships among magnitude, rupture length, rupture width, rupture area, and surface displacement. *Bull. Seismol. Soc. Am.* 84, 974–1002.
- Zapata, T., and Allmendinger, R. (1996). Thrust front zone of the Precordillera, Argentina: A thick-skinned triangle zone. *Bull. Am. Assoc. Petroleum Geol.* 80, 359–381.